PLOS ONE

RESEARCH ARTICLE

High-throughput analysis of lung immune cells in a combined murine model of agriculture dust-triggered airway inflammation with rheumatoid arthritis

Rohit Gaurav[1]*, Ted R. Mikuls[2,3], Geoffrey M. Thiele[2,3], Amy J. Nelson[1], Meng Niu[4], Chittibabu Guda[4], James D. Eudy[4], Austin E. Barry[1], Todd A. Wyatt[2,5,6,7], Debra J. Romberger[2,5], Michael J. Duryee[2,3], Bryant R. England[2,3], Jill A. Poole[1]

1 Division of Allergy and Immunology, Department of Internal Medicine, University of Nebraska Medical Center, Omaha, NE, United States of America, **2** Veterans Affairs Nebraska-Western Iowa Health Care System, Research Service, Omaha, NE, United States of America, **3** Division of Rheumatology & Immunology, Department of Internal Medicine, University of Nebraska Medical Center, Omaha, NE, United States of America, **4** Department of Genetics, Cell Biology and Anatomy, University of Nebraska Medical Center, Omaha, NE, United States of America, **5** Division of Pulmonary, Critical Care & Sleep, Department of Internal Medicine, University of Nebraska Medical Center, Omaha, NE, United States of America, **6** Department of Environmental, Agricultural & Occupational Health, College of Public Health, University of Nebraska Medical Center, Omaha, NE, United States of America, **7** Department of Internal Medicine, University of Nebraska Medical Center, Omaha, NE, United States of America

* rohit.gaurav@unmc.edu

Citation: Gaurav R, Mikuls TR, Thiele GM, Nelson AJ, Niu M, Guda C, et al. (2021) High-throughput analysis of lung immune cells in a combined murine model of agriculture dust-triggered airway inflammation with rheumatoid arthritis. PLoS ONE 16(2): e0240707. https://doi.org/10.1371/journal.pone.0240707

Editor: Michal A. Olszewski, University of Michigan Health System, UNITED STATES

Received: September 29, 2020

Accepted: December 18, 2020

Published: February 12, 2021

Peer Review History: PLOS recognizes the benefits of transparency in the peer review process; therefore, we enable the publication of all of the content of peer review and author responses alongside final, published articles. The editorial history of this article is available here: https://doi.org/10.1371/journal.pone.0240707

Data Availability Statement: The raw and analyzed data is deposited in the Gene Expression Omnibus (GEO) database with access number GSE155436.

Abstract

Rheumatoid arthritis (RA)-associated lung disease is a leading cause of mortality in RA, yet the mechanisms linking lung disease and RA remain unknown. Using an established murine model of RA-associated lung disease combining collagen-induced arthritis (CIA) with organic dust extract (ODE)-induced airway inflammation, differences among lung immune cell populations were analyzed by single cell RNA-sequencing. Additionally, four lung myeloid-derived immune cell populations including macrophages, monocytes/macrophages, monocytes, and neutrophils were isolated by fluorescence cell sorting and gene expression was determined by NanoString analysis. Unsupervised clustering revealed 14 discrete clusters among Sham, CIA, ODE, and CIA+ODE treatment groups: 3 neutrophils (inflammatory, resident/transitional, autoreactive/suppressor), 5 macrophages (airspace, differentiating/recruited, recruited, resident/interstitial, and proliferative airspace), 2 T-cells (differentiating and effector), and a single cluster each of inflammatory monocytes, dendritic cells, B-cells and natural killer cells. Inflammatory monocytes, autoreactive/suppressor neutrophils, and recruited/differentiating macrophages were predominant with arthritis induction (CIA and CIA+ODE). By specific lung cell isolation, several interferon-related and autoimmune genes were disproportionately expressed among CIA and CIA+ODE (e.g. *Oasl1*, *Oas2*, *Ifit3*, *Gbp2*, *Ifi44*, and *Zbp1*), corresponding to RA and RA-associated lung disease. Monocytic myeloid-derived suppressor cells were reduced, while complement genes (e.g. *C1s1* and *Cfb*) were uniquely increased in CIA+ODE mice across cell populations. Recruited and inflammatory macrophages/monocytes and neutrophils expressing interferon-, autoimmune-, and complement-related genes might contribute towards pro-fibrotic inflammatory

Funding: RG is supported by Central States Center for Agricultural Safety and Health NIOSH (U54OH010162). Study supported by grants from the National Institute of Environmental Health Sciences (R01ES019325 to JAP), National Institute for Occupational Safety and Health (U54OH010162 to JAP and TAW). TAW is the recipient of a Research Career Scientist Award (IK6 BX003781) from the Department of Veterans Affairs. TRM is supported by VA (CX000896 and BX004600) and grants from the National Institute of General Medical Sciences (U54GM115458) and the National Institute on Alcohol Abuse and Alcoholism (R25AA020818). BRE is supported by grants from the National Institute of General Medical Sciences (U54GM115458) and the Rheumatology Research Foundation. DJR is supported by VA Merit review 5I01CX001714-02. Study also supported by the Fred & Pamela Buffett Cancer Center Shared Resource, supported by the National Cancer Institute under award number P30CA036727. The University of Nebraska DNA Sequencing Core and Bioinformatics Core receive partial support from the National Institute for General Medical Science (NIGMS) NE-INBRE (Nebraska Research Network in Functional Genomics) (P20GM103427) and COBRE (1P30GM110768). This publication's contents are the sole responsibility of the authors. The funders had no role in study design, data collection and analysis, decision to publish, or preparation of the manuscript.

Competing interests: The authors have declared that no competing interests exist.

lung responses following airborne biohazard exposures in setting of autoimmune arthritis and could be predictive and/or targeted to reduce disease burden.

Introduction

Several lung diseases have been associated with rheumatoid arthritis (RA), including interstitial lung disease (ILD), chronic obstructive pulmonary disease (COPD), pulmonary nodules, pleural effusions, bronchiolitis obliterans, and asthma [1–3]. Affecting up to 40% or more of RA patients, RA-associated lung diseases pose a substantial burden to healthcare systems because of the increased morbidity and mortality, decreased quality of life, and tremendous healthcare costs [2, 4, 5]. Evidence of RA-related autoantibodies generated in lung mucosa, even in the absence of articular manifestations of RA [6], as well as increased concentrations of serum anti-citrullinated protein antibody accompanying RA-related lung diseases [1, 4, 7], reinforces the pathogenic links between pulmonary inflammation and autoimmunity leading to the development of RA. Therapeutic options for RA-associated lung disease are limited [8], and key cellular and/or mediators predictive of the development and/or progression of RA-associated lung disease are lacking [9]. Thus, studies are warranted to investigate and identify precise mechanisms underpinning these associations.

Exposure to environmental factors such as cigarette smoke represent shared risk factors in the development of RA and inflammatory lung diseases [3, 10]. However, insight into how inhalant injury might lead to or exacerbate RA and its pulmonary manifestations, has been limited in the absence of a relevant disease model. Recently a pre-clinical animal model to provide insight into the important cellular players and decipher molecular and potential mechanistic pathways involved in RA-associated inflammatory lung disease was established [11]. Specifically, the combination of the collagen-induced arthritis (CIA) model with a model of airborne biohazard exposure (e.g. agriculture related-organic dust extract/ODE) resulted in augmented arthritis inflammatory score and bone deterioration, increased systemic autoimmunity with increased anti-cyclic citrullinated peptide IgG antibodies, and promotion of pre-fibrotic inflammatory lung changes in mice [11] consistent with RA-associated lung disease pathophysiology. However, the mechanisms underlying these observations are not known. Here, we hypothesized that RA-associated lung disease is associated with unique cellular phenotypes and specific novel gene expression of *in vivo* exposed lungs. Leveraging this novel murine model, single-cell RNA sequencing (scRNA-seq) and unsupervised clustering were applied to lung immune cells among Sham, CIA, ODE, and CIA+ODE treatment groups to explore exposure-related differences in cellular subsets, transcriptional profiles, and associated biologic pathways. In separate complimentary studies to confirm key scRNA-seq findings, lung myeloid-derived cells (i.e. monocytes/macrophages and granulocytes) were isolated and subjected to gene-expression analysis.

Materials and methods

Animals

Arthritis prone DBA/1J male mice between 6–8 weeks of age were purchased from Jackson Laboratory (Bar Harbor, ME) and fed alfalfa-free chow *ad libitum* (Envigo Teklad, Huntingdon, Cambridgeshire, UK) as per supplier recommendations. All animal procedures were approved by the UNMC Institutional Animal Care and Use Committee (protocol #19-043-05) and were in accordance with NIH guidelines for the use of rodents and has been described

previously [11]. All procedures on mice were done under isofluorane to minimize distress. After every instillation or injection, animals were monitored consistently until they regained consciousness and mobility. They were monitored every day once by the investigators and once by the vivarium staff for any signs of discomfort or distress.

Organic dust extract

Organic dust extract (ODE) was prepared as previously reported [12] to model airway inflammatory disease. Briefly, an aqueous extract of organic dust from swine confinement feeding facilities (microbial-enriched agriculture setting) was prepared by incubating 1 g dust in 10 ml sterile Hank's Balanced Salt Solution (Mediatech, Manassas, VA) for 1 hour at room temperature followed by centrifugation for 10 minutes at 2,850 x g and repeated twice. The end supernate was filter-sterilized with a 0.22 μm syringe filter to remove any microorganisms and coarse particles. Constituents of the extract have been well characterized and include both endotoxin and peptidoglycans [11, 12]. ODE stock was prepared and stored at –20˚C in batches; aliquots were diluted for each experiment to a final concentration (vol/vol) of 12.5% in sterile phosphate buffered saline (PBS; pH = 7.4). Endotoxin concentrations ranged from 150–175 EU/mL as determined using the limulus amebocyte lysate assay (Lonza, Walkersville, MD). This concentration of ODE has been previously shown to produce optimal experimental effects and is well-tolerated in mice [11, 12].

Animal co-exposure model

The protocol for the co-exposure model has been previously described [11]. Briefly, mice were age-matched and randomized to 4 treatment groups: Sham (saline injection, saline inhalation), collagen-induced arthritis (CIA; CIA injection, saline inhalation), ODE (saline injection, ODE inhalation), and CIA + ODE (CIA injection, ODE inhalation). CIA was induced with two subcutaneous tail injections (100 μg) of chick type II collagen (2 mg/ml) emulsified in Freund's complete adjuvant (FCA) on day 1 and in Freund's incomplete adjuvant (IFA) on day 21. Sham injections and saline inhalation were conducted with sterile PBS. Following an established protocol, 50 μl of intranasal saline or 12.5% ODE daily for 5 weeks (weekends excluded) was used to induce airway inflammatory disease [11, 12]. Mouse treatment groups were ran in parallel with euthanization occurring 5 weeks after initiation of treatments.

Arthritis evaluation

Arthritis inflammatory scores were assessed weekly using the semiquantitative, mouse arthritis scoring system provided by Chondrex (www.chondrex.com) as previously described [11]. Scores range from 0 (no inflammation) to 4 (erythema and severe swelling encompassing ankle, foot, and digits). Arthritis evaluation was assessed on 8 mice per treatment group from 3 independent studies.

Lung histopathology

Lung sections of Sham, CIA, ODE, and CIA+ODE treatment groups previously obtained [11] were stained with H&E or with anti-CD3 (1:100, Cat#ab5690, Lot#GR3356033-2), anti-CD68 (1:50, Cat#ab31630, Lot#GR3305929-3), and anti-MPO (1:25, Cat#ab9535, Lot#GR331736-4) from Abcam (Cambridge, MA), anti-CD45R (1:40, Cat#14-0452-82, Lot#2178350) from Invitrogen (Grand Island, NY), and anti-CCR2 (1:100, Cat# NBP267700, Lot# HMO537) from Novus Biologicals (Centennial, CO). Cross absorbed (H+L) goat anti-rabbit (Cat#A32731, Lot#UK290266), goat anti-mouse (Cat#A32727, Lot#UL287768) and goat-anti rat

(Cat#A21434, Lot#2184321) from Thermo Fisher, Grand Island, NY) were used at 1:100 dilution as secondary antibodies. Slides were mounted with VECTASHIELD® Antifade Mounting Medium with DAPI (Cat#H-1200, Lot#ZG1014, Burlingame, CA) and visualized under Zeiss fluorescent microscope.

Single-cell RNA sequencing

For these studies, 2 mice per treatment group were euthanized with isoflurane in a desiccator. Lungs were exposed from the thoracic cavity and perfused with 10 ml heparin-PBS [11]. Harvested lungs were dissociated with gentleMACS dissociator (Miltenyi Biotech, Auburn, CA) in a digestion solution (collagenase I, 0.2 μg/μl + DNase I, 75 U/ml + heparin, 1.5 U/ml, in Dulbecco's Modified Eagle's Media; DMEM) and incubated for 30 minutes at 37˚C in a shaking incubator. Digestion solution activity was neutralized with PBS containing 4 mM EDTA. Red blood cells were lysed with 1 ml ammonium-chloride-potassium (ACK) lysis buffer (Quality Biological, Gaithersburg, MD) for 1 minute and neutralized with ice-cold DMEM (Gibco). Cells were processed for RNAseq in FACS buffer (2% fetal bovine serum (FBS) + 0.1% NaN_3 in PBS). All reagents purchased from Sigma unless otherwise specified.

Single cell suspensions generated from whole lung were quantified and viability tested using a LUNA-FL™ Dual Fluorescence Cell Counter (Logos Biosystems, Annandale, VA). Single cells were then isolated from cell suspensions (100–2,000 cells/μl) using a 10x Chromium controller per manufacturer's suggested protocol (10x Genomics, Pleasanton, CA). Following cell capture, the gel beads in emulsion (GEM)/sample solution was recovered and placed into strip tubes. Reverse transcription was performed on a thermocycler (C1000 Touch™ Thermal Cycler, Bio-Rad, Hercules, CA) per recommended protocol followed by cDNA amplification. Amplified products were solid phase reversible immobilization (SPRI) bead-purified and evaluated by Fragment Analyzer (Agilent, Santa Clara, CA). Twenty-five percent of the cDNA volume was subjected to fragmentation and double-sided SPRIselect (Beckman Coulter, Indianapolis, IN) was used for PCR purification and clean-up. After adaptor ligation, SPRI clean-up was performed and PCR amplification using sample specific indexes for each sample was completed. PCR products were purified, quantified and library size distribution determined by Fragment Analyzer. Libraries were sequenced per the manufacturer's suggested parameters on a NextSeq500 sequencer to an average depth of 50,000 reads per cell.

Single-cell RNA sequencing data processing

Basecall files (BCL) were generated through 10xGenomics Chromium Single cell 3' Solution followed by RNA Sequencing using Nextseq 500 and Nextseq 550. *Cellranger mkfastq* was used for demultiplexing and to convert BCL files into FASTQ files. FASTQ files were run through *Cellranger count* to perform alignment (using STAR aligner), filtering, and unique molecular identifier (UMI) counting. Chromium cellular barcodes were used to generate gene-barcode matrices, perform clustering, and do gene expression analyses. *Cellranger aggr* was used to normalize and pool the results from different samples, followed by the application of Principal Components Analysis (PCA) to change the dimensionality of the datasets. t-SNE (t-Stochastic Neighbor Embedding) was used to visualize the data in a 2-D space. Graph-based unsupervised clustering was then used to cluster the cells. We used Loupe browser [13], R packages including cellranger R-kit [14], complex heatmap [15], and Geom_violin [16] for more in-depth analysis to compare genes expression in each cluster compared to all the other clusters and plot the data. The data sets have been deposited to the Gene Expression Omnibus (GEO) database with access number GSE155436.

Lung cell sorting

In separate studies with 8 mice per treatment group from 3 independent studies and following mouse euthanasia and lung perfusion, lungs were inflated with 1 ml digestion solution/mouse containing 0.5 mg/ml Liberase^{TM} (medium Thermolysin concentration; Millipore Sigma, St. Louis, MO) and 235.5 U/ml DNAse I in Hank's Balanced Salt Solution (pH = 7.2). Inflated lungs were dissociated with gentleMACS dissociator (Miltenyi Biotech, Auburn, CA) and incubated for 15 minutes at 37˚C in a shaking incubator. Digestion solution activity was neutralized with FA3 buffer (10mM HEPES, 2mM EDTA, 1% FBS in PBS). The single cell lung suspensions were incubated with CD16/32 (Fc Block, Cat#101320, Lot#B276722) Biolegend, San Diego, CA) to minimize nonspecific antibody staining. Next, cells stained with mAbs directed against rat anti-mouse CD45 (clone 30-F11, Cat#563053, Lot#8330943), Ly6C (clone AL-21, Cat#560596, Lot#9267106), Ly6G (clone 1A8, Cat#551461, Lot#21331), CD11b (clone M1/70, Cat#550993, Lot#8232762), and hamster anti-mouse CD11c (clone N418, Cat#61-0114-82, Lot#2133313, Invitrogen, Eugene, OR), and live/dead fixable blue dead cell stain kit (Invitrogen, Eugene, OR). Antibodies to CD11c from Invitrogen, and the remainder from BD Biosciences (San Jose, CA). Flow-sorting was done with FACSAria II (BD Biosciences). Live $CD45^+$ singlets were gated on $Ly6C^+Ly6G^+$ to sort neutrophils. Lymphocytes (based on FSC and SSC) and neutrophils (based on Ly6C and Ly6G staining) were then reverse gated to further select for 3 monocyte/macrophage populations: macrophage ($CD11c^{high}$, $CD11b^{variable}$), monocytes-macrophages ($CD11c^{intermediate}$,$CD11b^{high}$), and monocytes ($CD11c^-$, $CD11b^{high}$). This gating strategy for monocyte/macrophage populations is consistent with previous reports by us and others [17–20].

RNA isolation

The 4 cell-sorted populations were counted, assessed for viability by trypan blue exclusion (>95%), washed and lysed with RLT buffer containing β-mercaptoethanol for RNA isolation as per manufacturer's instructions with Qiagen RNAeasy Micro Kit (Qiagen, Germantown, MD).

NanoString nCounter system

Quality and quantity of total RNA was evaluated using a Fragment Analyzer (Agilent, Santa Clara, CA) and Nanodrop (ThermoFisher), respectively. Total RNA (25–50 ng) was hybridized and processed per the manufacturer's suggested protocol with capture and reporter probes to prepare target-probe complexes using reagents from the Mouse Autoimmune profiling panel containing 771 genes (NanoString, Seattle, WA). Complexes were purified, immobilized and aligned on a cartridge for counting on the nCounter system and processed as per the manufacturer's instructions.

For NanoString analyses, three independent studies of 2–3 pooled mice per group/experiment (N = 8 total mice/group) were analyzed by ANOVA with Tukey's multiple comparisons test. Arthritis inflammatory scores over time was also analyzed by ANOVA. Gene expression data were normalized to 20 housekeeping genes, treatment groups (CIA, ODE and CIA +ODE) were compared to Sham, and data plotted as fold-change. ANOVA with Tukey's multiple comparison test was used on myeloid-derived suppressor cell (MDSC) posthoc analysis. Bar graphs were used to depict means with standard errors of the ratio change in MDSCs normalized to Sham (percentile of MDSC treatment group divided by percentile of MDSC Sham group). Statistical analyses were performed using the GraphPad Prism software, version 8.4.3 (GraphPad, San Diego, CA), and statistical significance accepted at p-values <0.05.

Results

Agriculture (swine) exposure-related ODE-induced airway inflammation coupled with arthritis modeling

Consistent with the previously published study describing this model system [11], the highest arthritis inflammatory scores were demonstrated for CIA+ODE at 5 weeks (Fig 1A). Throughout the 5 weeks, arthritis inflammatory scores were recorded weekly, and as early as 1 week, there were increases in arthritis inflammatory scores in CIA+ODE and CIA alone as compared with Sham. At 4 weeks, there were significant increases in ODE alone. Previous lung pathology investigations [11] reported increases in alveolar and bronchiolar compartment inflammation and increases in cellular aggregates with ODE and CIA+ODE as compared to Sham, but the number and size of cellular aggregates were reduced in CIA+ODE as compared to ODE alone. Instead, pro-lung fibrosis mediators including lung hyaluronan and fibronectin were increased in CIA+ODE as compared to ODE alone [11]. In these current studies, lung sections from the previous study were stained with H&E from each treatment group showing increased inflammation in CIA+ODE (Fig 1B). Sections were also stained with markers to identify macrophages (CD68), neutrophils (MPO), T cells (CD3), and B cells (CD45R) (Fig 1C and 1D) distributed in the parenchyma, peribronchiolar and perivascular region. Infiltration of recruited $CCR2^{+}$ inflammatory monocytes was also demonstrated in the CIA and ODE groups, and these cells were further potentiated in the CIA+ODE group (Fig 1E and 1F).

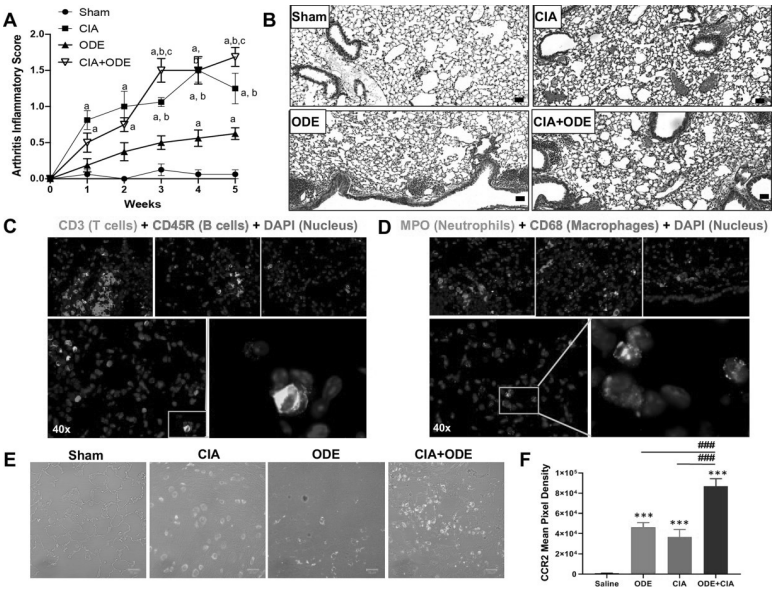

Fig 1. Agriculture (swine) exposure-related Organic Dust Extract (ODE) induced airway inflammation coupled with Collagen Induced Arthritis (CIA) model. (**A**) Line graph depicts mean with SE bars of arthritis inflammatory score at respective time points from treatment groups. Statistical difference versus sham denoted as "a" ($p<0.05$); versus ODE denoted "b" ($p<0.05$); versus CIA denoted as "c" ($p<0.05$) as determined by two-way ANOVA. N = 8 mice/group from 3 independent studies. (**B**) Representative H&E-stained lung section from each treatment group at 10 X magnification with line scale (100 pixels). Representative images of lungs of CIA+ODE at 40x (parenchyma and peribronchiolar/perivascular regions), immunostained with CD3 (T cells) and CD45R (B cells) (**C**), and myeloperoxidase (MPO, neutrophils) and CD68 (macrophages) (**D**). Zoomed images highlight B-cell-T-cell interaction (**C**) and macrophages with neutrophils (**D**). CCR2+ inflammatory monocytes were increased with ODE and CIA treatment conditions in murine lungs. (**E**) Representative image of CCR2 expression (yellow) of lung tissue from each treatment group. (**F**) Bar graph depicts mean with standard error bars of CCR2 staining (N = 5/group). Statistical difference $^{***}p<0.001$ vs. saline/sham control and ###$p<0.001$ denoted by line between groups.

https://doi.org/10.1371/journal.pone.0240707.g001

These studies lay the foundation for current studies delineating cellular and gene determinations through high-throughput analysis.

ScRNA-seq identifies 14 unique immune cell subsets

The 10x genomics platform was utilized to cumulatively capture all lung cells. In total, 16,822 cells were analyzed with a mean of 42,901 post-normalization reads per cell and 956 median genes per cell. Unsupervised clustering was performed on 11,577 $CD45^+$ cells and plotted on *t*-distributed Stochastic Neighbor Embedding (t-SNE). Projection of cells was colored based on unique molecular identifier (UMI) count to identify level of transcripts among the cells. The average UMI count range was roughly between 2,000 to 12,000. Cells that were distributed in the middle showed the highest level of transcripts while cells at the top showed the lowest level (Fig 2A). Unsupervised clustering on the t-SNE projected cells revealed 14 unique immune cell subsets coded by different colors and arbitrary numbers (Fig 2B). Clusters 3, 4 and 8 were identified as neutrophil subsets based on distribution of *Csf3r* (granulocyte colony stimulating factor receptor [21]) in t-SNE analysis (Fig 2C). Macrophages were distributed in the middle and were identified with *Cd11c* (ITGAX) expression in clusters 1, 2, 5, 11, 14, and partially in cluster 10. Monocytes (inflammatory monocytes) were identified with *F13a1* expression in cluster 12. Cluster 9 showed high levels of *Ccl5* expression suggesting the presence of NK cells. Similarly, *Cd19* expressing cells in cluster 7 identified B lymphocytes, and *Trbc2* expression in clusters 6 and 13 identified T lymphocytes, along with expression in the NK cell population (cluster 9). Dendritic cells (DCs) were located in cluster 10 and were characterized by *Siglech* expression, particularly evident in cluster 10a (Fig 2C).

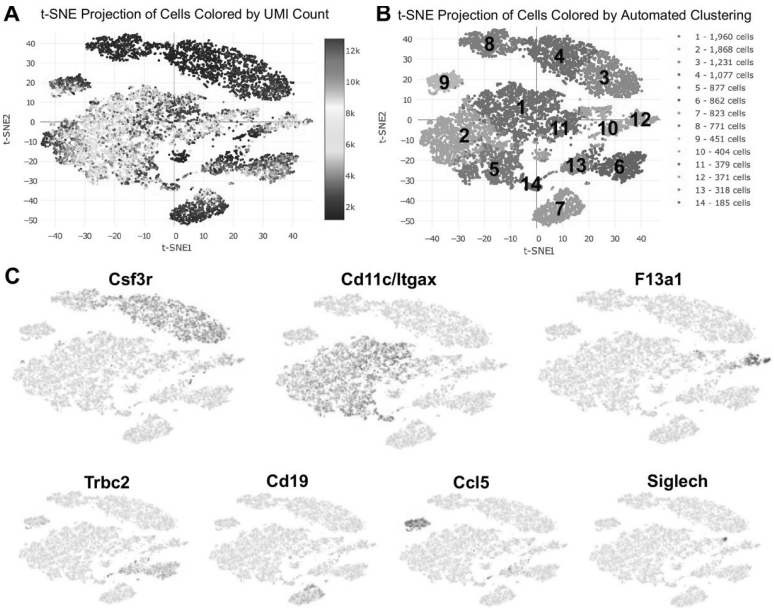

Fig 2. Unsupervised single-cell transcriptional profiling of lung $CD45^+$ cells identifies 14 unique clusters among Sham, CIA, ODE, and CIA+ODE treatment groups. Lung immune cells were isolated from mice (N = 2 mice/group) treated with Sham, CIA, ODE and CIA+ODE. (**A**) T-distributed stochastic neighbor embedding (*t-SNE*) plot shows projection of unique molecular identifier (UMI) count among cell clusters. (**B**) Distribution of cells by unsupervised clustering in *t-SNE* showing lung immune cell populations. (**C**) Major lung cell types identified by signature genes including *Csf3r* (neutrophils), *Cd11c/Itgax* (macrophages), *F13a1* (monocytes), *Trbc2* (T lymphocytes), *Cd19* (B lymphocytes), *Ccl5* (NK cells), and *Siglech* (dendritic cells).

https://doi.org/10.1371/journal.pone.0240707.g002

CIA and ODE drive unique distributions of immune cells within identified clusters

The 4 treatment groups (Sham, CIA, ODE, and CIA+ODE) exhibited unique distributions of lung immune cells among the identified clusters (Fig 3A and 3B). Among the neutrophil clusters, Sham was exclusively represented by cluster 4, but not cluster 3 or 8. In contrast, the CIA group almost entirely showed neutrophil distribution in cluster 3. The ODE group demonstrated selective distribution of neutrophils in cluster 8 with overlap into cluster 4. In the combination exposure CIA+ODE group, there was broader distribution of neutrophils with predominance in cluster 3, but also evidence for distribution in cluster 4 and partially in cluster 8 (Fig 3A and 3B).

Based on the shifts observed in the cell populations among treatment groups, a manual sub-clustering was performed to delineate exact number of cells distributed among the sub-clusters (Fig 3C). Among the macrophage clusters, the ODE group had prevalence in clusters 5, 1b and 1c compared to the CIA group. Likewise, the ODE group lacked clusters 1a and 2a. A subset of cluster 12 (12b) and cluster 10 (10b) were [22] unique to the CIA group, while clusters 10a and 12a were unique to the ODE group (Fig 3). The combination group with CIA+ODE showed a mixed population representing CIA and ODE, while leaning more towards the CIA group (Fig 3).

Lymphocyte populations were confined to clusters 6, 7, 9, and 13, and were represented in all treatment groups, although modest shifts in cell population distribution were observed. Particularly, NK cells (cluster 9) and B cells (cluster 7) were differentially expressed in ODE and CIA treatment groups with apparent shifts from cluster 9a in ODE to cluster 9b in CIA and shifts from cluster 7a in ODE to cluster 7b in CIA, respectively (Fig 3). Similar to the macrophage clusters, the CIA+ODE group portrayed CIA and ODE group while inclining more towards the CIA group (Fig 3).

Three distinct neutrophil populations revealed by scRNA-seq among treatment groups

Unsupervised clustering segregated 3 populations of granulocytes/neutrophils that were marked by unique gene expression (Fig 4A). Relative gene-expression compared to all other cell populations as log2 fold-change was plotted in a heat map (Fig 4B) and violin plot (Fig 4C) to compare transcript levels as well as cell distributions at different expression levels. Cluster 8 showed increased expression of inflammatory genes such as *Ccl3*, *Ccl4*, *Cxcl2*, *Upp1* and *Marcks1* (log2 fold-change range: 4.98–6.35), which are genes commonly upregulated in

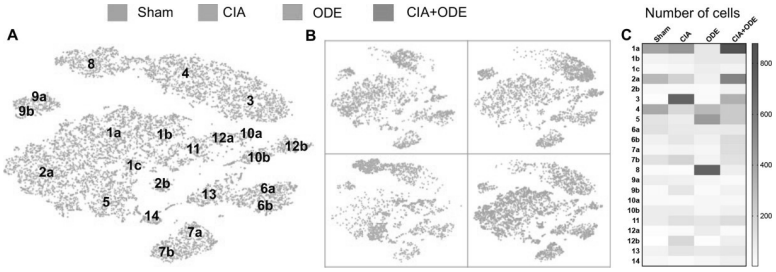

Fig 3. Distribution of aggregated gene clusters among treatment groups. Sham, CIA, ODE and CIA+ODE treatment groups demonstrate differences in cell distribution among 14 gene clusters. Sham is represented by red, CIA by green, ODE by teal, CIA+ODE by blue. (**A**) tSNE plot with all the treatment groups merged with respective colors (**B**) Treatment groups are plotted individually with their respective colors to show cell distribution. (**C**) Heatmap shows number of cells per sub-cluster among treatment groups by manual sub-clustering (total cells = 11,577).

https://doi.org/10.1371/journal.pone.0240707.g003

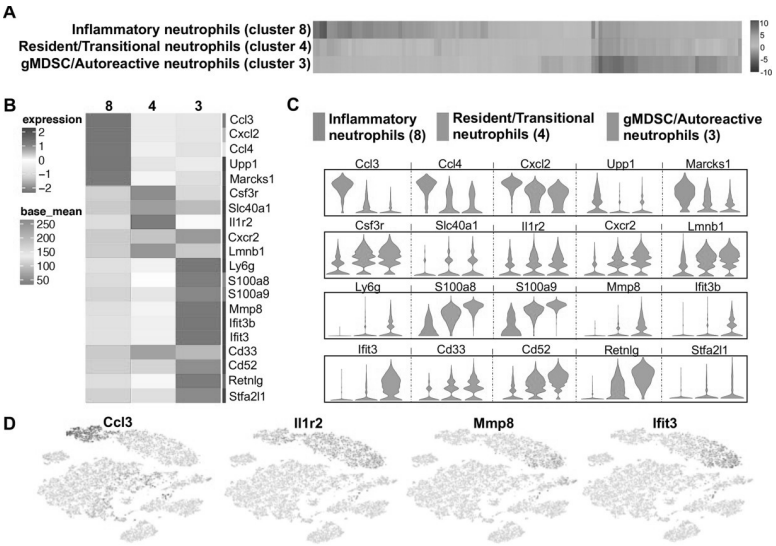

Fig 4. Neutrophil populations segregated by unsupervised clustering relate to cell-programming among treatment groups. (**A**) Heatmap shows the top 120/N upregulated genes for 3 distinct neutrophil clusters ranked by log2 fold-change, where N = total number of clusters. (**B**) Top 5–10 genes of the three neutrophil clusters plotted in heatmap to show differences and gene names in transcript levels. (**C**) Violin plots show expression with population distribution among inflammatory neutrophils, represented by blue (cluster 8), resident/transitional neutrophils, represented by green (cluster 4) and granulocytic myeloid-derived suppressor cells (gMDSC)/autoreactive neutrophils, represented by red (cluster 3). The y-axis indicates normalized expression value, log2 (average UMI count + 1). (**D**) Representative gene from each neutrophil cluster showing their distribution in t-SNE.

https://doi.org/10.1371/journal.pone.0240707.g004

activated neutrophils (Fig 4B and 4C, and S1 Table) [23–27]. Moreover, cluster 8 was exclusive to the ODE group. In contrast, cluster 3 exhibited increased expression of genes associated with immunosuppression and autoreactivity as well as genes that are characteristic of granulocytic MDSC (gMDSC) such as *S100a8*, *S100a9*, *Mmp8*, *Ifit3b*, *Ifit3*, *Cd33*, *Cd52* and *Stfa2l1* (log2 fold-change range: 5.16–6.03) (Fig 4B and 4C, and S1 Table) [28–34]. Based on the gene expression profiles, cluster 8 was identified as "inflammatory neutrophils" and cluster 3 was identified as "gMDSC/autoreactive neutrophils". Intermediate to the two cell subsets, another neutrophil subset (cluster 4) was identified as resident/transitional neutrophils. This population of neutrophils (Fig 4B and 4C, and S1 Table) demonstrated increased expression of *Csf3r*, *Il1r2*, *Slc40a1*, *Cxcr2*, and *Lmnb1* genes (log2 fold-change range: 3.91–4.24) that are required in neutrophil differentiation and trafficking [21, 35–40]. Neutrophils in the CIA+ODE group was distributed more like the CIA than the ODE group with predominant segregation in clusters 3 and 4 (Fig 3).

Signature genes were selected to highlight respective neutrophil populations on the t-SNE plot (Fig 4D). *Ccl3* was selected to highlight "inflammatory neutrophil" as *Ccl3* enhances recruitment and activation of neutrophils in a paracrine fashion [23, 24]. Because *Il1r2* gene encodes for type 2 interleukin-1 receptor and is constitutively expressed in mouse neutrophils [35], it identified all subsets of neutrophils in the t-SNE clusters (Fig 4D). Autoreactive neutrophils/gMDSCs were exclusively positive for *Mmp8* and *Ifit3* in t-SNE. *Mmp8* is a neutrophil collagenase [41, 42] and *Ifit3* codes for interferon induced protein with tetratricopeptide repeats 3, as both are highly upregulated in gMDSCs and can suppress immune response [31, 32].

Identification of unique macrophage/monocyte/DC populations

Based on gene expression patterns among segregated populations found with unsupervised clustering, 5 discrete macrophage clusters, 1 inflammatory monocyte cluster, and 1 DC cluster

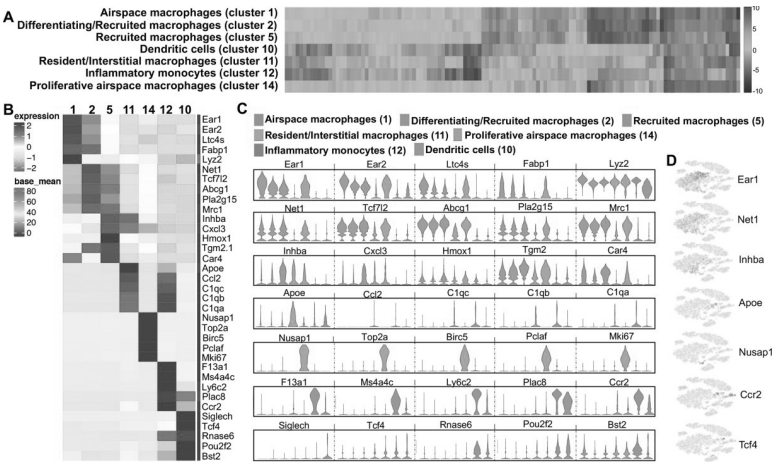

Fig 5. Differences in transcript levels among monocyte-macrophages and dendritic cell (DC) populations. (**A**) Heatmap shows the top 120/N upregulated genes for 7 macrophages/monocytes and DC clusters ranked by log2 fold-change, where N = total number of clusters. (**B**) Heatmap showing differences among top 5 genes with gene names of the macrophages/monocytes and DC populations. (**C**) Expression levels with violin plots among airspace macrophages (red, cluster 1), differentiating/recruited macrophages (brown, cluster 2), recruited macrophages (green, cluster 5), resident/interstitial macrophages (teal, cluster 11), proliferative airspace macrophages (light blue, cluster 14), inflammatory monocytes (lavender, cluster 12), dendritic cells (pink, cluster 10). The y-axis indicates normalized expression value, log2 (average UMI count + 1). (**D**) Distribution of respective cell populations by a representative gene in t-SNE plot.

https://doi.org/10.1371/journal.pone.0240707.g005

were identified (Fig 5A). Cluster 1 was termed "airspace macrophages" based on increased expression (log2 fold-change range: 1.52–1.98) of *Ear1*, *Ear2*, *Ltc4s*, *Fabp1* and *Lyz2* compared to other clusters (Fig 5B–5D), representing genes responsible for metabolism and inflammation/resolution [43–47] (S2 Table). Cluster 2 was labeled as "differentiating/recruited macrophages" as this cluster exhibited the highest expression (log2 fold-change range: 1.27–1.54) of *Net1*, *Tcf7l2*, *Abcg1*, *Pla2g15* and *Mrc1* representing genes implicated in differentiation, antigen uptake, and macrophage recruitment [48–52] (Fig 5B–5D). Cluster 2 macrophages expressed genes associated with alternatively activated macrophages (M2 macrophages) [49, 52], and upregulate pathways for lipoprotein metabolism and redox signaling (S2 Table). Cluster 5 was identified as "recruited macrophages" based on the disproportionate expression (log2 fold-change range: 1.5–1.96) of *Inhba*, *Cxcl3*, *Hmox1*, *Tgm2*, and *Car4* (Fig 5B–5D). Cluster 5 was heterogeneous with *Inhba* representing classically activated (M1) macrophages or *Hmox1* as M2 macrophages, and also included genes that are involved in inflammation, adipogenesis, homeostasis and phagocytosis [53–62] (S2 Table).

Sham, CIA and CIA+ODE groups showed similar distribution of airspace (particularly cluster 1a) and recruited macrophages (especially cluster 2a) while the ODE group had a substantial reduction in these macrophage populations with segregation towards the center of the t-SNE plot in clusters 1b and 1c (Fig 3).

Cluster 11 was designated as "resident interstitial macrophages" with high transcript levels of *Apoe*, *Ccl2* and complement genes such as *C1qc*, *C1qb* and *C1qa* (Fig 5B–5D) ranging from log2 fold-change of 3.54–3.91. This population also displayed heterogeneity with expression of both M1 and M2 genes [47, 63–67] involved in inflammation and resolution (S2 Table). Resident interstitial macrophages were more evident in the ODE compared to other treatment groups (Fig 3).

As reported by Mould *et. al.* [68], we also identified a distinct cluster of macrophages (cluster 14) with very high expression of proliferative and mitotic genes (log2 fold-change range:

5.79–8.12) including *Nusap1*, *Top2a*, *Birc5*, *Pclaf*, and *Mki67* (Fig 5B–5D), which were termed "proliferative airspace macrophages." The upregulated pathways included cell-cycle, mitosis or proliferation-related pathways (S2 Table) [68–70]. These proliferative airspace macrophages were represented largely by the ODE and CIA+ODE groups (Fig 3).

Cluster 12 represented a unique cell population identified as "inflammatory monocytes." This population exhibited increased expression of *F13a1*, *Ms4a4c*, *Ly6c2*, *Plac8* and *Ccr2* (Fig 5B–5D) (log2 fold-change range: 4.65–6.53), all characteristically expressed in inflammatory monocytes and often correlated with anti-viral and/or autoimmune responses [71–79]. Although CIA+ODE group had a pronounced cluster 12, 12b represented the CIA group and ODE group exhibited cluster 12a (Fig 3). A cell population in cluster 10 was identified demonstrating elevated expression in genes (log2 fold-change range: 2.61–6.48) of *Siglech*, *Tcf4*, *Rnase6*, *Pou2f2* and *Bst2* (Fig 5B–5D), which are distinctive of DCs [80–86]. This population demonstrated characteristics of plasmacytoid DCs involving genes associated with innate immunity and anti-inflammatory pathways. The DC predominated with ODE and CIA+ODE groups in cluster 10a, whereas cluster 10b predominated with Sham (Fig 3). Overall, CIA +ODE group distribution of monocyte-macrophages followed neutrophils with overrepresentation of CIA group (Fig 3).

Lymphocytes segregate in four clusters among treatment groups

Four discrete lymphocyte clusters were found in the analysis (Fig 6A). Cluster 6 was identified as "T lymphocytes", with increased expression (log2 fold-change range: 4.87–7.04) of *Lef1*, *Igfbp4*, *Tcf7*, *Cd3d*, and *Cd3e* (Fig 6B–6D). This population favored type 2 $CD4^+$ cells based upon the expression of differentiating or expanding population of T lymphocytic genes [87–91]. Cluster 6a was more represented by Sham whereas cluster 6b was represented by CIA and CIA+ODE treatment groups. The ODE group had sparse distribution between cluster 6a and 6b (Fig 3). In contrast to cluster 6, cluster 13 exhibited increased expression of genes indicative of activated T lymphocytes including *Icos*, *Thy1*, *Cd3g*, *Ikzf2* and *Maf* (log2 fold-change range: 4.87–5.87) and thus were termed as "effector T lymphocytes" (Fig 6B–6D) with upregulation

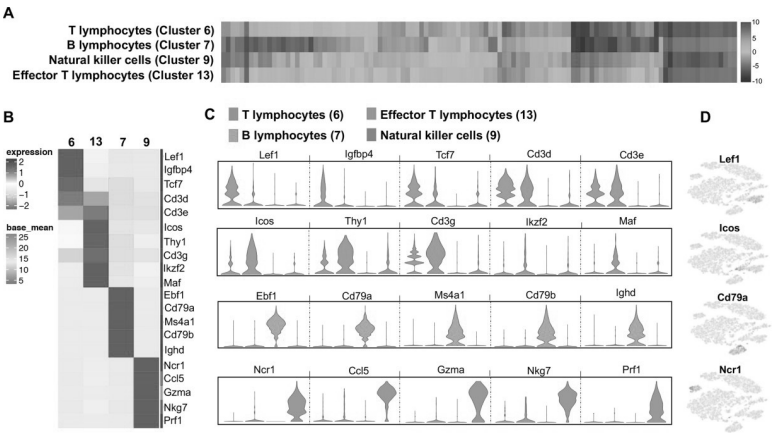

Fig 6. Four discrete lymphocyte populations suggest heterogeneity among treatment groups. (**A**) Heatmap shows the top 120/N upregulated genes for 5 distinct lymphocyte clusters ranked by log2 fold-change, where N = total number of clusters. (**B**) The top 5 genes with gene names of each lymphocyte cluster are shown in heatmap. (**C**) Violin plots show variability in transcript levels among cell populations including T lymphocytes (red, cluster 6), effector T lymphocytes (green, cluster 13), B lymphocytes (teal, cluster 7) and natural killer cells (lavender, cluster 9). The y-axis indicates normalized expression value, log2 (average UMI count + 1). (**D**) Representative genes from each cluster show their distribution in t-SNE plot.

https://doi.org/10.1371/journal.pone.0240707.g006

of co-stimulatory and adaptive immune pathways. Subtle differences were observed in the distribution of activated T lymphocytes among the treatment groups (Fig 3).

Cluster 7 was remarkable for increased gene expression characteristic of B lymphocytes such as *Ebf1*, *Cd79a*, *Ms4a1*, *Cd79b* and *Ighd* (log2 fold-change range: 7.29–7.77) (Fig 6B–6D). Along with genes implicated in B-cell differentiation, memory, signaling and autoimmunity, this cluster showed striking similarities with upregulated pathways in the T lymphocyte population (S3 Table) [92–95]. B lymphocytes had an overall distribution in CIA+ODE group, but largely represented as cluster 7b in the CIA group. The ODE group had very few B lymphocytes with sparse distribution (Fig 3).

NK cell-specific gene expression was increased in cluster 9 with *Ncr1*, *Ccl5*, *Gzma*, *Nkg7* and *Prf1* (Fig 6B–6D) ranging from 7.83 to 7.87 log2 fold-change (S3 Table). These genes and pathways were predominately related to NK cell recruitment, activation and effector function [96–101]. The Sham and ODE groups were represented by cluster 9a while the CIA group had more of cluster 9b. The CIA+ODE group had 9a and 9b clusters (Fig 3).

Differential gene expression of ex vivo sorted lung neutrophils across treatment groups represent disease progression

To understand the relevance of myeloid-derived lung cells in RA and RA-associated lung disease, these studies sought to determine whether gene expression of sorted lung myeloid-derived cells corresponded to disease-specific findings among treatment groups. Lung neutrophils were isolated by fluorescence activated cell sorting (FACS) based on traditional cell surface markers as percent of $CD45^+$ cells that were $Ly6C^+$ $Ly6G^{high}$ (Fig 7A and S1 Fig). Sham represented resident neutrophils in the lungs at baseline [102]. By NanoString analysis, upregulated genes of isolated neutrophils resembled the gene expression demonstrated in scRNA-seq data by respective treatment groups. Neutrophils isolated from lungs of CIA and CIA +ODE groups (as compared to Sham) demonstrated increased transcript levels of genes

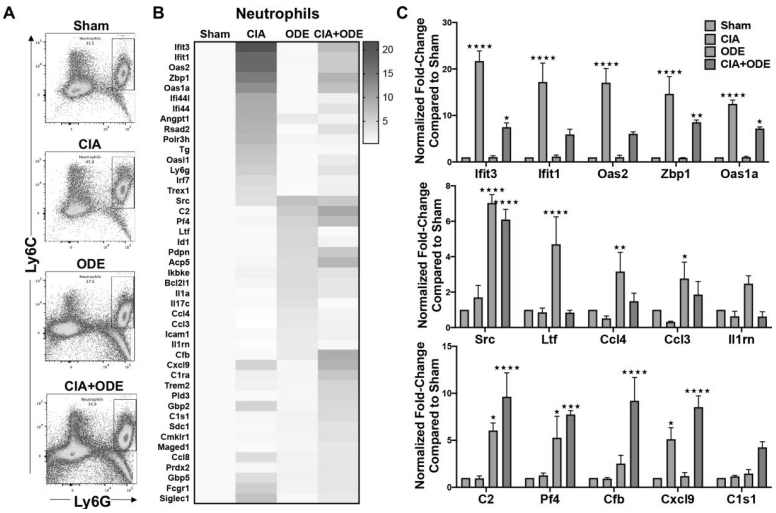

Fig 7. Treatment group-specific gene expression pattern demonstrated in isolated lung neutrophils. Neutrophils were sorted from lung digests as live, singlets, $CD45^+$, non-lymphocytes, $Ly6C^+$ and $Ly6G^+$. (**A**) Representative dot plots of $Ly6C^+$ $Ly6G^+$ neutrophils sorted from Sham, CIA, ODE and CIA+ODE treatment groups shown. (**B**) Heat map of fold-change of top 15 genes normalized to 20 housekeeping genes from each treatment group compared to Sham. (**C**) Bar graphs reflect the mean of normalized fold-change with standard error bars of representative genes from each treatment group Sham (red), CIA (green), ODE (teal), and CIA+ODE (blue). N = 3 (3 independent experiments with 2–3 mice pooled, 8 total mice). $^*P<0.05$, $^{**}P<0.01$, $^{***}P<0.001$, $^{****}P<0.0001$.

https://doi.org/10.1371/journal.pone.0240707.g007

involved in autoimmunity as well as genes associated with gMDSCs/autoreactive neutrophils. These included (CIA and CIA+ODE): *Ifit3* (21.7 and 7.49-fold), *Ifit1* (17.2 and 5.9-fold), *Oas2* (17.0 and 6.0-fold), *Zbp1* (14.6 and 8.5-fold), *Cxcl9* (5.1 and 8.5-fold), and *Oas1a* (12.5 and 7.2-fold) (Fig 7B and 7C). Interestingly, the CIA+ODE group also showed gene expression that paralleled that of the ODE group, including increased transcript levels of *Src* (CIA+ODE: 6.1-fold and ODE: 7-fold), *Pf4* (7.7 and 5.3-fold), and complement cascade genes such as *C2* (9.6 and 6-fold-change), and *Cfb* (9.2 and 2.5-fold-change) (Fig 7B and 7C). In contrast, the ODE group demonstrated exclusive upregulation of *Ltf* (4.7-fold-change), *Ccl4* (3.2-fold), *Ccl3* (2.8-fold) and *Il1rn* (2.5-fold) as compared to Sham, consistent with the inflammatory neutrophil cluster (Fig 7B and 7C). There was a single complement cascade gene (*C1s1*) that was exclusively upregulated in CIA+ODE (4.3-fold) (Fig 7C).

Macrophage and monocyte populations from CIA and CIA+ODE groups exhibit gene profiles comparable to RA and RA-associated lung disease, respectively

After excluding dead cells, doublets, lymphocytes and neutrophils (Ly6G^{-}), 3 separate lung monocyte-macrophage populations were sorted based upon CD11c and CD11b expression (Fig 8A and S1 Fig) [17, 18]. These 3 populations are 1) CD11c^{high}CD11b^{variable} macrophages, 2) CD11c^{intermediate}CD11b^{high} mono-macs and 3) CD11b^{high}CD11c^{-} monocytes. Of the CD11c^{high} macrophages, the expression of CD11b (evident on the pseudocolor plots; Fig 8A) shifts to the right: CIA+ODE>ODE>CIA as compared to Sham. Increasing expression of CD11b on CD11c+ macrophages suggest an activated phenotype [18, 103]. Infiltrating inflammatory monocytes and recruited monocytes/macrophages have been implicated in other experimental lung fibrotic experimental settings [104–106]. Similar to neutrophils, the isolated

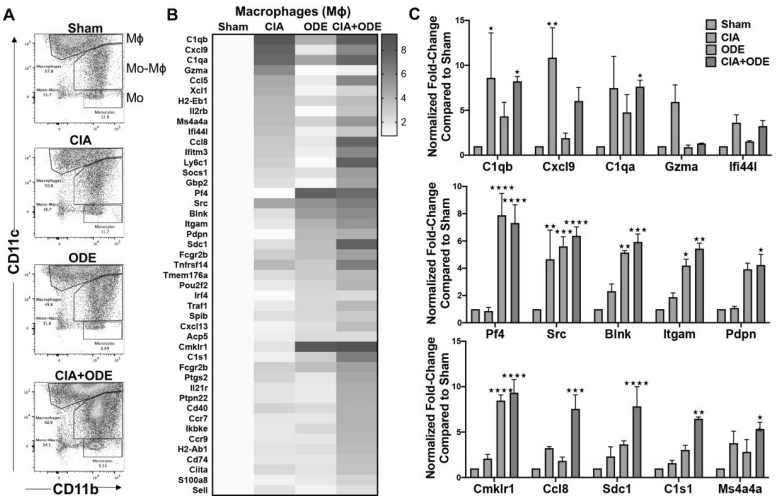

Fig 8. Treatment group-specific gene expression pattern demonstrated in isolated macrophages. Three monocyte/macrophage populations were sorted from lung digests as live, singlets, CD45^{+}, non-lymphocytes, Ly6C^{-} and Ly6G^{-}, and identified as separate populations with variable expression of CD11b and CD11c. RNA was isolated from these populations and subjected to NanoString nCounter analysis. (**A**) Representative dot plots of the populations sorted as: (1) macrophages (CD11c^{high}, CD11b^{variable}), (2) monocytes-macrophages (CD11c^{intermediate},CD11b^{high}), and (3) monocytes (CD11c^{-}, CD11b^{high}) from each treatment of Sham, CIA, ODE, and CIA+ODE shown. (**B**) Heat map of fold-change of top 15 genes normalized to 20 housekeeping genes from each treatment group compared to Sham. (**C**) Bar graphs depict mean with standard error bars of representative genes from each treatment group Sham (red), CIA (green), ODE (teal), and CIA+ODE (blue). N = 3 (3 independent experiments with 2–3 mice pooled), 8 total mice. *P<0.05, **P<0.01, ***P<0.001, ****P<0.0001.

https://doi.org/10.1371/journal.pone.0240707.g008

macrophage population also demonstrated increased gene expression in CIA and CIA+ODE group that included *C1qb* (8.6 and 8.2-fold), *Cxcl9* (10.9 and 6-fold), *C1qa* (7.5 and 7.6-fold), *Ifi44l* (3.6 and 3.2-fold), *Cmklr1* (2.1 and 9.3-fold), *Ccl8* (3.2 and 7.6-fold), *Sdc1* (2.3 and 7.8-fold), and *Ms4a4a* (3.8 and 5.3-fold). Increased expression of *Gzma* was unique to the CIA group (6-fold) (Fig 8B and 8C), while *C1s1* was upregulated in both CIA+ODE (6.5-fold) and ODE (3-fold) groups along with *Pf4* (7.9 and 7.3-fold), *Itgam* (4.2 and 5.4-fold), and *Pdpn* (4 and 4.2-fold). Expression of *Src* (4.7, 5.6 and 6.4-fold) and *Blnk* (2.3, 5.1 and 5.9-fold) was increased in all treatment groups (CIA, ODE and CIA+ODE) as compared to Sham (Fig 8B and 8C).

The $CD11c^{intermediate}CD11b^{+}$ monocyte-macrophage population demonstrated increased expression of several interferon-associated and other genes implicated in autoimmune responses in CIA and CIA+ODE groups including *Gbp2* (7.4 and 6.9-fold), *Zbp1* (7 and 2-fold), *Ifi44* (6.6 and 4.3-fold), *Ifi44l* (6 and 5.1-fold), *Cxcl9* (5.8 and 8.1-fold), and *Fcgr1* (2.4 and 2.9-fold). ODE and CIA+ODE groups demonstrated increased expression of *Cxcl5* (3.4 and 2.6-fold), *Pdpn* (4.2 and 3.3-fold), *Pf4* (5.4 and 3.8-fold), and *Cxcl13* (6.8 and 3.6-fold) compared to Sham (Fig 9A and 9B). *Cfb* (5.9, 4.1, and 16.3-fold), *Ccl8* (11.3, 5.1, and 6.7-fold), and *C1s1* (5.8, 7, and 19.3-fold) were overexpressed in CIA, ODE and CIA+ODE groups, respectively, compared to Sham. Expression of non-canonical I-kappa-B kinase, *Ikbke*, associated with anti-viral responses and autoimmune diseases, was increased in the CIA+ODE group (2.5-fold) compared to Sham (Fig 9A and 9B).

The monocyte population ($CD11c^{-}CD11b^{+}$) was unique because all the upregulated genes including *Oasl1* (15 and 4.6-fold), *Oas1a* (15.6 and 15.3-fold), *Oas2* (11.7 and 12.4-fold), *Ifi44* (11.0 and 9.5-fold), *Ifi44l* (11.1 and 11.1-fold), *Siglec1* (11.1 and 6.1-fold), *Gbp2* (2.9 and 5.3-fold), *Gbp5* (3.8 and 4.3-fold), *Stat1* (3.3 and 3.8-fold), and *Isg15* (4.1 and 3.7-fold) were increased in both CIA and CIA+ODE groups respectively (Fig 10A and 10B). Moreover, these

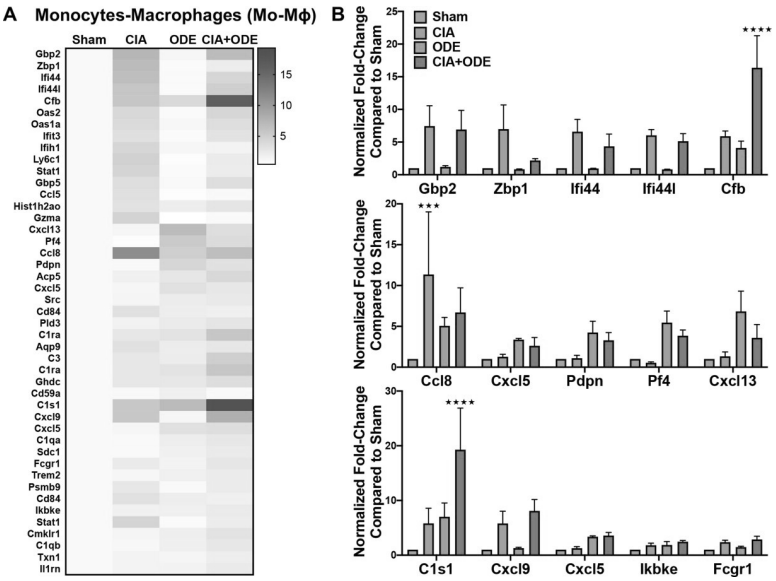

Fig 9. Treatment group-specific gene expression pattern demonstrated is isolated monocyte-macrophage population. Monocytes-macrophages were sorted as $CD11c^{intermediate}$,$CD11b^{high}$. (**A**) Heat map of fold-change of top 15 genes/treatment group (CIA, ODE and CIA+ODE) normalized to 20 housekeeping genes compared to Sham. (**B**) Bar graphs of mean with standard error bars of representative genes from each treatment group Sham (red), CIA (green), ODE (teal), and CIA+ODE (blue). N = 3 (3 independent experiments with 2–3 mice pooled, 8 total mice). $^{***}P<0.001$, $^{****}P<0.0001$.

https://doi.org/10.1371/journal.pone.0240707.g009

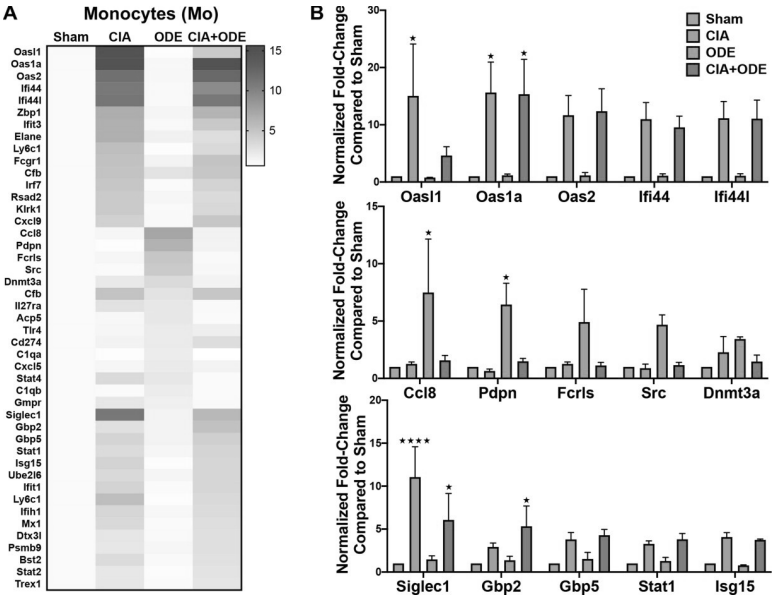

Fig 10. Treatment group-specific gene expression pattern. Demonstrated in isolated monocytes. Monocytes were sorted as CD11c^{-}, CD11b^{high}. (**A**) Heat map of fold-change of top 15 genes/treatment group (CIA, ODE and CIA +ODE) normalized to 20 housekeeping genes compared to Sham. (**B**) Bar graphs depict mean with standard error bars of representative genes from each treatment group Sham (red), CIA (green), ODE (teal), and CIA+ODE (blue). N = 3 (3 independent experiments with 2–3 mice pooled, 8 total mice). *P<0.05, ****P<0.0001.

https://doi.org/10.1371/journal.pone.0240707.g010

genes are mostly associated with autoimmunity or immunosuppression [32, 57]. The ODE group exhibited higher transcript levels of *Ccl8* (7.5-fold), *Pdpn* (6.4-fold), *Fcrls* (4.9-fold) and *Src* (4.7-fold), consistent with the other sorted neutrophil and monocytes/macrophages populations. While *Cfb* expression was increased in all 3 treatment groups, *Dnmt3a* was upregulated (2.3 and 3.4-fold) in ODE and CIA+ODE groups, respectively (Fig 10A and 10B), but not in CIA.

Finally, gMDSCs were identified as Ly6C^{+}Ly6G^{high}CD11b^{high}SSC^{high} (S2 Fig) [107, 108] on posthoc gating of sorted neutrophil populations resulting in non-significant variations across the treatment groups (Fig 11A). In contrast, mMDSC defined as Ly6G^{-} CD11b^{+} Ly6C^{high} SSC^{low} cells (S2 Fig) [107, 108] were increased with CIA but decreased with ODE and CIA +ODE (Fig 11B).

Discussion

In this study, scRNA-seq analysis was applied to whole lung immune cells from a mouse model of RA-associated inflammatory lung disease with key findings confirmed in sorted lung cell populations and NanoString analysis. Building upon the preclinical model of RA-associated inflammatory lung disease [11], we report a number of key findings in this study including: (a) identification of 3 unique neutrophil populations including inflammatory, transient and immunosuppressive/autoreactive granulocytes among experimental groups, (b) heterogeneity among 5 macrophage populations including metabolically active, proliferative, differentiating, recruited, and residential with classical (M1) and alternatively (M2)-activated genes, (c) identification of 2 stages of T-lymphocytes (differentiating and effector), a B-cell population and a NK cell cluster, (d) variability in the distribution of cellular clusters among the treatment groups representing RA and RA-associated lung disease (CIA and CIA+ODE groups, respectively), (e) identification of gMDSC and mMDSC populations based on cell surface markers,

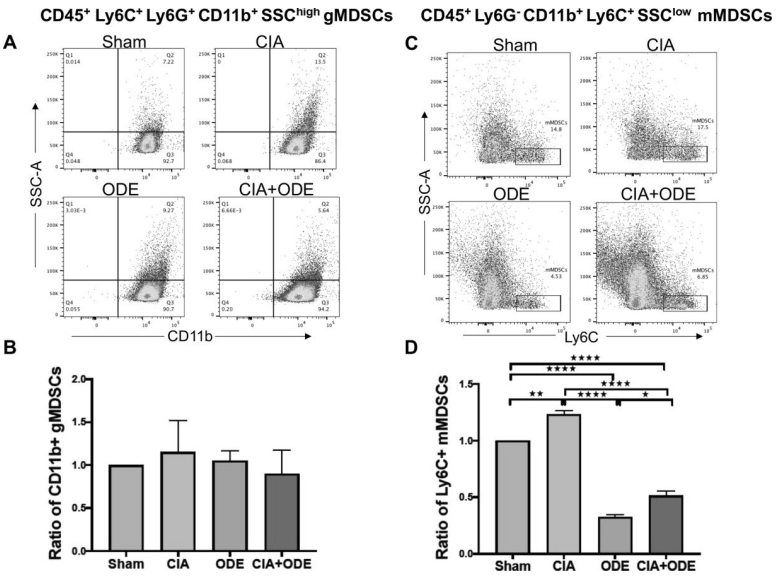

Fig 11. Differences in myeloid-derived suppressor cells (MDSCs) identified in posthoc analysis among treatment groups. (**A**) Dot plots show differences in $CD45^+$ $Ly6C^+$ $Ly6G^+$ $CD11b^+$ SSC^{high} granulocytic (g) MDSCs among treatment groups. (**B**) Bar graph depicts mean with standard error bars of the ratio change in gMDSCs as normalized to Sham (percentile of gMDSC treatment group divided by percentile of gMDSC Sham group). (**C**) Dot plots show differences in $CD45^+$ $Ly6G^-$ $CD11b^+$ $Ly6C^+$ SSC^{low} monocytic (m) MDSCs among treatment groups. (**D**) Bar graph depicts mean with standard error bars of the ratio change in mMDSCs as normalized to Sham (percentile of mMDSC treatment group divided by percentile of mMDSC Sham group). N = 3 (3 independent experiments with 2–3 mice pooled; 8 total mice). $^*P<0.05$, $^{**}P<0.01$, $^{****}P<0.0001$.

https://doi.org/10.1371/journal.pone.0240707.g011

and (f) identification of unique genes (interferon-related/autoimmune and complement cascade) that are found in a mouse model of RA-associated inflammatory lung disease.

Occupational exposures from farming, construction, mechanics, medical and military waste have been associated with increased risk of development of RA and/or RA-associated lung disease [109–113]. However, precise mechanism(s) of the development of RA-associated lung disease with occupational and/or environmental inflammatory exposures is not known. Working towards identifying these mechanisms, previous studies demonstrated that repeated exposure to microbial-enriched ODE and particularly ODE+CIA increases citrullination and malondialdehyde-acetaldehyde (MAA)-adduction of lung proteins with a corresponding increase in circulating autoantibody concentrations, periarticular bone damage, and increased deposition of extracellular matrix proteins with a reduction in classical airway inflammatory markers [11, 114]. These findings suggested a transition of inflammatory lung disease towards a pro-fibrotic phenotype. Leveraging this co-exposure mouse model with CIA and ODE, several immune cell populations exhibiting unique gene expression signatures that were differentially distributed across treatment groups were demonstrated that suggest potential roles in the pathogenesis of RA, inflammatory lung disease, and inflammatory lung disease specific to RA.

Neutrophils have been classically related to inflammation and host response to pathogens [115]. Knowledge of their role in inflammation and homeostasis continues to evolve as various subsets of neutrophils have been identified and proposed based upon steady state, inflammatory, or anti-inflammatory programming [116]. Many intermediate phenotypes have also been defined, further complicating classifications and the proposed roles in both disease and homeostasis [117]. The 3 different neutrophil populations currently identified aptly signify an inflammatory (in ODE), anti-inflammatory (or autoreactive) (in CIA and CIA+ODE) and homeostatic (transient) (in Sham). In the cell sorting/NanoString studies, neutrophils were

identified and limited to Ly6C$^+$ Ly6G$^+$ cells based upon equipment limitations of simultaneous 4-cell capture ability. Future studies to include the Ly6G$^+$ Ly6C$^-$ cells that were predominately observed with ODE and CIA+ODE could also be informative. Further studies are needed to delineate precisely how these sub-populations program the lung immune response towards inflammatory and pro-fibrotic disease states.

MDSCs have been implicated in RA [118] as well as ILD [119]. However, their relationship to the RA-associated lung disease is not well-established. MDSCs are transient populations representing myeloid cells at various stages of differentiation that suppress immunity and are subdivided into granulocytic (g) or monocytic (m) origin [120–122]. MDSCs are identified by their high expression of *Nox2*, calprotectin (*S100a8*/*S100a9*), *Mmp8*, *Mmp9*, *Cd33*, and multiple interferon-inducible genes such as *Ifit3*, *Ifit1*, *Oas2*, *Zbp1*, *Ifi44*, *Ifi44l* and *Oas1a* [123, 124]. By scRNA-seq analysis, resolution of gMDSC was high with population segregation in cluster 3, which was driven by systemic arthritis induction (i.e. CIA and CIA+ODE groups). This finding was further strengthened by the RNA analysis of the sorted Ly6G$^+$ Ly6C$^+$ neutrophil population of corresponding treatment groups. Posthoc analysis confirmed that the sorted group contained gMDSCs with Ly6G$^+$ Ly6C$^+$ CD11b^{high} SSC^{high} gating [107, 108], but there was no difference across treatment groups. Unsupervised clustering of immune cells did not segregate mMDSCs. However, gene expression of sorted monocyte-macrophage populations based on CD11b and CD11c expression suggested the presence of mMDSC-like properties based upon the immunosuppressive genes that were elevated in CIA and CIA+ODE groups. Using a classical gating strategy (Ly6G$^-$ CD11b$^+$ Ly6C^{high} SSC^{low}) for mMDSCs [108], mMDSCs were identified with FACS and found to be decreased in combination (CIA+ODE) exposure group. These findings are consistent with a recent report that showed that the expansion of MDSCs following tofacitinib treatment is inversely related to the progression of ILD in the SKG mouse model of RA-ILD [125]. These collective findings would suggest a potential protective role for lung MDSCs (particularly mMDSCs) in the development RA-related lung disease, and future studies are warranted to understand their role in disease manifestations to potentially develop novel targets for therapeutic interventions.

Macrophages are one of the most versatile immune cells with immense population heterogeneity and diverse functions [126, 127]. Macrophages are increasingly appreciated for their role in fibrosis, wound repair and resolution [47, 68, 128]. In this current study, the metabolically active airspace macrophages, resident, recruited and differentiating macrophages (clusters 1, 11, 5 and 2, respectively) contribute to inflammation and resolution, while the proliferative airspace macrophages (cluster 14) signify self-renewing properties to maintain a steady population in the lungs. These studies potentially open avenues for hypothesis generation based on various non-traditional genes (interferon-related/autoimmune and complement cascade) expressed in the macrophage subsets that have not been previously investigated in health and disease. The unique distribution of various macrophage clusters among the treatment groups, particularly clusters 1b, 1c, 5 and 11 in ODE group, and clusters 1a, 2a and 12b (inflammatory monocytes) in CIA and CIA+ODE groups signify their importance in disease transition from RA to RA-associated lung disease. Correspondingly, infiltrative CCR2$^+$ inflammatory monocytes were demonstrated with CIA and ODE with highest expression in combined exposures. Future studies could determine whether targeting this cell population results in a reduction of disease manifestations.

Subtle differences among lymphocyte populations (clusters 6, 7, 9 and 13) support earlier work demonstrating that B lymphocytes are skewed towards an autoreactive response following airborne biohazard exposure [114]. B lymphocytes have been recognized as one of the major drivers of autoimmunity [129] and are the target of highly effective RA therapies such as rituximab [130]. Colocalization of MAA with autoreactive B lymphocytes in lung tissues of

RA-ILD patients [131] further signifies their potential role in the pathogenesis of RA-ILD. While NK cells are considered a bridge between innate and adaptive immune responses [132], targeting cluster 9b could be of interest. Similarly, autoreactive T lymphocytes (perhaps cluster 6b) and cellular phenotypes supporting fibroproliferation with increase in activated fibroblasts with extracellular matrix deposition could be of particular interest in RA-ILD.

In addition to confirming the upregulation of several interferon-induced genes implicated in autoimmunity, complement cascade genes such as *C1ra*, *C1qa*, *C1qb*, *C2*, and *Cfb* representing classical and alternative pathways [133] were identified. *C1s1* was highlighted among the complement cascade genes due to its high expression, and was invariably upregulated in the CIA+ODE group in all 4 cell-sorted neutrophil and monocyte-macrophage populations. *C1* acts as a sensor for self and non-self-recognition and thus plays a major role in self-tolerance [134]. Complement cascade genes are recognized in RA [135] and ILD [136–138], but remain overlooked as therapeutic targets [139]. Holers *et. al.* [135] suggested that RA-ILD has a complement connection, but to our knowledge, this is among the first reports to experimentally identify *C1s1* or complement cascade genes in a RA-inflammatory lung disease model.

There are limitations of this study. In general, animal modeling of arthritis-lung disease interactions are overall limited. The over-expressing TNF-alpha transgenic mice that develop an array of connective tissue diseases has been associated with interstitial lung disease and pulmonary hypertension, particularly in female mice [22]. The arthritic SKG mice develop a cellular and fibrotic interstitial pneumonia [140], but SKG mice do not develop compelling evidence of autoimmunity or arthritis following inhalation injury (i.e tobacco smoke or bleomycin) [140]. Our model system utilizing complex agriculture dust exposure-induced airway inflammation in the setting of CIA would be representative of populations whereby inhalant airborne toxicants are recognized risk factors for RA and RA-lung disease. Cigarette smoke exposure is the most-well-environmental established risk for RA, and occupational inhalant exposures (e.g. work exposures in farming, construction, mining, warehouse environments) have been increasingly associated with risk of disease development, particularly among men [112, 141, 142]. Moreover, it has previously been reported that ODE exposure induced citrullinated and malondialdehyde-acetaldehyde (MAA) modified proteins in the lung tissue [114], antigens that have been implicated in RA pathogenesis. The advantage of this modeling system is that disease development is dependent on airborne biohazard exposures and can be readily modified to investigate other types of exposures. These current studies were focused on male mice because previous work demonstrated that male mice were profoundly more susceptible to CIA+ODE induced adverse effects as compared to female mice [11]. Moreover, it is also recognized that non-arthritic male mice are susceptible to inhalant endotoxin-induced bone loss whereas female mice were protected and that this protection was dependent upon estrogen [143]. Future studies may be warranted to investigate how single airborne biohazard exposures (e.g. endotoxin, pollutants) in the setting of arthritis induction affect lung-arthritis disease as well as specific hormone factors including testosterone, progesterone, and estrogen. Although lung DCs were noted to be limited in this mouse modeling system, future studies could also investigate the role of lung DCs in lung inflammatory disorders associated with RA.

In conclusion, application of scRNA-seq to an animal model combining systemic arthritis induction and environmental inhalant-induced lung inflammation (i.e. RA-associated lung disease) identified unique populations of lung immune cell clusters differentially ascribed to individual treatment conditions. Neutrophil subpopulations and heterogeneous macrophage-monocyte populations were identified in addition to unique genes (interferon-related and complement cascade) that could be contributing to the pathogenesis of RA-associated lung disease. Additionally, this information might inform potential candidates that could be

exploited in future investigations examining targeted interventions and the identification of informative disease biomarkers.

Supporting information

S1 Fig. Gating strategy for FACS-based population isolation. Neutrophils were sorted from lung digests as live, singlets, $CD45^+$, non-lymphocytes, $Ly6C^+$ and $Ly6G^+$. Three monocyte/macrophage populations were sorted from lung digests as live, singlets, $CD45^+$, non-lymphocytes, $Ly6C^-$and $Ly6G^-$, and identified as separate populations with variable expression of CD11b and CD11c as: (1) macrophages ($CD11c^{high}$, $CD11b^{variable}$), (2) monocytes-macrophages ($CD11c^{intermediate}$,$CD11b^{high}$), and (3) monocytes ($CD11c^-$, $CD11b^{high}$).
(TIF)

S2 Fig. Gating strategy for posthoc analysis of myeloid-derived suppressor cells (MDSCs). Granulocytic (g) MDSCs were identified as live, singlets, $CD45^+$, non-lymphocytes that were $Ly6C^+$ $Ly6G^+$ $CD11b^+$ SSC^{high}. Whereas monocytic (m) MDSCs were identified as live, singlets, $CD45^+$, non-lymphocytes that were $Ly6G^-$ $CD11b^+$ $Ly6C^+$ SSC^{low}.
(TIF)

S1 Table. The top 10 genes uniquely identified to neutrophil subtypes with mean UMI count, log2 fold-change and adjusted p value as compared to all other CD45+ lung cell clusters.
(PDF)

S2 Table. The top 10 genes uniquely identified to monocyte, macrophage and DC subtypes with average UMI count, log2 fold-change and adjusted p value compared to all other CD45+ lung cell clusters.
(PDF)

S3 Table. The top 10 genes uniquely identified to lymphocytes subtypes with average UMI count, log2 fold-change and adjusted p value compared to all other CD45+ lung cell clusters.
(PDF)

Acknowledgments

We thank Victoria B. Smith, Samantha D. Wall, Craig L. Semerad in the Flow Cytometry Research Facility at UNMC for technical support for flow cytometry studies. We thank Jennifer L. Bushing in the Sequencing Core at UNMC for assistance with NanoString studies. We also thank Lisa R. Chudomelka for article preparation assistance and submission.

Author Contributions

Conceptualization: Rohit Gaurav, Ted R. Mikuls, Geoffrey M. Thiele, Michael J. Duryee, Bryant R. England, Jill A. Poole.

Data curation: Rohit Gaurav, Amy J. Nelson, Meng Niu, James D. Eudy, Austin E. Barry.

Formal analysis: Rohit Gaurav, Meng Niu, Chittibabu Guda, James D. Eudy.

Funding acquisition: Ted R. Mikuls, Chittibabu Guda, James D. Eudy, Bryant R. England, Jill A. Poole.

Investigation: Rohit Gaurav, Jill A. Poole.

Methodology: Rohit Gaurav, Amy J. Nelson, Meng Niu, Chittibabu Guda, James D. Eudy.

Resources: Chittibabu Guda, Jill A. Poole.

Software: Meng Niu, Chittibabu Guda, James D. Eudy.

Supervision: Chittibabu Guda, Jill A. Poole.

Validation: Rohit Gaurav, Jill A. Poole.

Visualization: Rohit Gaurav.

Writing – original draft: Rohit Gaurav, Jill A. Poole.

Writing – review & editing: Rohit Gaurav, Ted R. Mikuls, Geoffrey M. Thiele, Amy J. Nelson, Meng Niu, Chittibabu Guda, James D. Eudy, Austin E. Barry, Todd A. Wyatt, Debra J. Romberger, Michael J. Duryee, Bryant R. England, Jill A. Poole.

References

1. Aubart F, Crestani B, Nicaise-Roland P, Tubach F, Bollet C, Dawidowicz K, et al. High levels of anti-cyclic citrullinated peptide autoantibodies are associated with co-occurrence of pulmonary diseases with rheumatoid arthritis. J Rheumatol. 2011; 38(6):979–82. https://doi.org/10.3899/jrheum.101261 PMID: 21362759
2. Shaw M, Collins BF, Ho LA, Raghu G. Rheumatoid arthritis-associated lung disease. Eur Respir Rev. 2015; 24(135):1–16. https://doi.org/10.1183/09059180.00008014 PMID: 25726549
3. Friedlander HM, Ford JA, Zaccardelli A, Terrio AV, Cho MH, Sparks JA. Obstructive lung diseases and risk of rheumatoid arthritis. Expert Rev Clin Immunol. 2020; 16(1):37–50. https://doi.org/10.1080/1744666X.2019.1698293 PMID: 31774329
4. Salaffi F, Carotti M, Di Carlo M, Tardella M, Giovagnoni A. High-resolution computed tomography of the lung in patients with rheumatoid arthritis: Prevalence of interstitial lung disease involvement and determinants of abnormalities. Medicine (Baltimore). 2019; 98(38):e17088. https://doi.org/10.1097/MD.0000000000017088 PMID: 31567944
5. Raimundo K, Solomon JJ, Olson AL, Kong AM, Cole AL, Fischer A, et al. Rheumatoid Arthritis-Interstitial Lung Disease in the United States: Prevalence, Incidence, and Healthcare Costs and Mortality. J Rheumatol. 2019; 46(4):360–9. https://doi.org/10.3899/jrheum.171315 PMID: 30442831
6. Janssen KM, de Smit MJ, Brouwer E, de Kok FA, Kraan J, Altenburg J, et al. Rheumatoid arthritis-associated autoantibodies in non-rheumatoid arthritis patients with mucosal inflammation: a case-control study. Arthritis Res Ther. 2015; 17:174. https://doi.org/10.1186/s13075-015-0690-6 PMID: 26155788
7. Perry E, Eggleton P, De Soyza A, Hutchinson D, Kelly C. Increased disease activity, severity and autoantibody positivity in rheumatoid arthritis patients with co-existent bronchiectasis. Int J Rheum Dis. 2017; 20(12):2003–11. https://doi.org/10.1111/1756-185X.12702 PMID: 26200759
8. Cassone G, Manfredi A, Vacchi C, Luppi F, Coppi F, Salvarani C, et al. Treatment of Rheumatoid Arthritis-Associated Interstitial Lung Disease: Lights and Shadows. J Clin Med. 2020; 9(4). https://doi.org/10.3390/jcm9041082 PMID: 32290218
9. Wang D, Zhang J, Lau J, Wang S, Taneja V, Matteson EL, et al. Mechanisms of lung disease development in rheumatoid arthritis. Nat Rev Rheumatol. 2019; 15(10):581–96. https://doi.org/10.1038/s41584-019-0275-x PMID: 31455869
10. Anderson R, Meyer PW, Ally MM, Tikly M. Smoking and Air Pollution as Pro-Inflammatory Triggers for the Development of Rheumatoid Arthritis. Nicotine Tob Res. 2016; 18(7):1556–65. https://doi.org/10.1093/ntr/ntw030 PMID: 26957528
11. Poole JA, Thiele GM, Janike K, Nelson AJ, Duryee MJ, Rentfro K, et al. Combined Collagen-Induced Arthritis and Organic Dust-Induced Airway Inflammation to Model Inflammatory Lung Disease in Rheumatoid Arthritis. J Bone Miner Res. 2019; 34(9):1733–43. https://doi.org/10.1002/jbmr.3745 PMID: 30995344
12. Poole JA, Wyatt TA, Oldenburg PJ, Elliott MK, West WW, Sisson JH, et al. Intranasal organic dust exposure-induced airway adaptation response marked by persistent lung inflammation and pathology in mice. Am J Physiol Lung Cell Mol Physiol. 2009; 296(6):L1085–95. https://doi.org/10.1152/ajplung.90622.2008 PMID: 19395665

13. 10x Genomics. What is Loupe Browser? 2020 [Available from: https://support.10xgenomics.com/single-cell-gene-expression/software/visualization/latest/what-is-loupe-cell-browser.

14. Genomics x. Cell Ranger R Kit Tutorial: Secondary Analysis on 10x Genomics Single Cell 3' RNA-seq PBMC Data 2017 [updated 18 July. Available from: http://cf.10xgenomics.com/supp/cell-exp/cellrangerrkit-PBMC-vignette-knitr-2.0.0.pdf.

15. Gu Z, Eils R, Schlesner M. Complex heatmaps reveal patterns and correlations in multidimensional genomic data. Bioinformatics. 2016; 32(18):2847–9. https://doi.org/10.1093/bioinformatics/btw313 PMID: 27207943

16. Hintze JL, Nelson R. D. Violin Plots: A Box Plot-Density Trace Synergism. The American Statistician. 1998; 52(2):181–4.

17. Redente EF, Keith RC, Janssen W, Henson PM, Ortiz LA, Downey GP, et al. Tumor necrosis factor-alpha accelerates the resolution of established pulmonary fibrosis in mice by targeting profibrotic lung macrophages. Am J Respir Cell Mol Biol. 2014; 50(4):825–37. https://doi.org/10.1165/rcmb.2013-0386OC PMID: 24325577

18. Poole JA, Nordgren TM, Heires AJ, Nelson AJ, Katafiasz D, Bailey KL, et al. Amphiregulin modulates murine lung recovery and fibroblast function following exposure to agriculture organic dust. Am J Physiol Lung Cell Mol Physiol. 2020; 318(1):L180–L91. https://doi.org/10.1152/ajplung.00039.2019 PMID: 31693392

19. Kirby AC, Raynes JG, Kaye PM. CD11b regulates recruitment of alveolar macrophages but not pulmonary dendritic cells after pneumococcal challenge. J Infect Dis. 2006; 193(2):205–13. https://doi.org/10.1086/498874 PMID: 16362884

20. Lee J, Boyce S, Powers J, Baer C, Sassetti CM, Behar SM. CD11cHi monocyte-derived macrophages are a major cellular compartment infected by Mycobacterium tuberculosis. PLoS Pathog. 2020; 16(6): e1008621. https://doi.org/10.1371/journal.ppat.1008621 PMID: 32544188

21. Basheer F, Rasighaemi P, Liongue C, Ward AC. Zebrafish Granulocyte Colony-Stimulating Factor Receptor Maintains Neutrophil Number and Function throughout the Life Span. Infect Immun. 2019; 87(2):e00793–18. https://doi.org/10.1128/IAI.00793-18 PMID: 30455199

22. Bell RD, White RJ, Garcia-Hernandez ML, Wu E, Rahimi H, Marangoni RG, et al. Tumor Necrosis Factor Induces Obliterative Pulmonary Vascular Disease in a Novel Model of Connective Tissue Disease-Associated Pulmonary Arterial Hypertension. Arthritis Rheumatol. 2020.

23. Hartl D, Krauss-Etschmann S, Koller B, Hordijk PL, Kuijpers TW, Hoffmann F, et al. Infiltrated neutrophils acquire novel chemokine receptor expression and chemokine responsiveness in chronic inflammatory lung diseases. J Immunol. 2008; 181(11):8053–67. https://doi.org/10.4049/jimmunol.181.11.8053 PMID: 19017998

24. Sokol CL, Luster AD. The chemokine system in innate immunity. Cold Spring Harb Perspect Biol. 2015; 7(5):a016303. https://doi.org/10.1101/cshperspect.a016303 PMID: 25635046

25. Tang BM, Shojaei M, Teoh S, Meyers A, Ho J, Ball TB, et al. Neutrophils-related host factors associated with severe disease and fatality in patients with influenza infection. Nat Commun. 2019; 10 (1):3422. https://doi.org/10.1038/s41467-019-11249-y PMID: 31366921

26. El Amri M, Fitzgerald U, Schlosser G. MARCKS and MARCKS-like proteins in development and regeneration. J Biomed Sci. 2018; 25(1):43. https://doi.org/10.1186/s12929-018-0445-1 PMID: 29788979

27. Sheats MK, Pescosolido KC, Hefner EM, Sung EJ, Adler KB, Jones SL. Myristoylated Alanine Rich C Kinase Substrate (MARCKS) is essential to beta2-integrin dependent responses of equine neutrophils. Vet Immunol Immunopathol. 2014; 160(3–4):167–76. https://doi.org/10.1016/j.vetimm.2014.04.009 PMID: 24857637

28. Sinha P, Okoro C, Foell D, Freeze HH, Ostrand-Rosenberg S, Srikrishna G. Proinflammatory S100 proteins regulate the accumulation of myeloid-derived suppressor cells. J Immunol. 2008; 181 (7):4666–75. https://doi.org/10.4049/jimmunol.181.7.4666 PMID: 18802069

29. Yang J, Anholts J, Kolbe U, Stegehuis-Kamp JA, Claas FHJ, Eikmans M. Calcium-Binding Proteins S100A8 and S100A9: Investigation of Their Immune Regulatory Effect in Myeloid Cells. Int J Mol Sci. 2018; 19(7):1833. https://doi.org/10.3390/ijms19071833 PMID: 29933628

30. Uhel F, Azzaoui I, Gregoire M, Pangault C, Dulong J, Tadie JM, et al. Early Expansion of Circulating Granulocytic Myeloid-derived Suppressor Cells Predicts Development of Nosocomial Infections in Patients with Sepsis. Am J Respir Crit Care Med. 2017; 196(3):315–27. https://doi.org/10.1164/rccm.201606-1143OC PMID: 28146645

31. Taleb K, Auffray C, Villefroy P, Pereira A, Hosmalin A, Gaudry M, et al. Chronic Type I IFN Is Sufficient To Promote Immunosuppression through Accumulation of Myeloid-Derived Suppressor Cells. J Immunol. 2017; 198(3):1156–63. https://doi.org/10.4049/jimmunol.1502638 PMID: 28003378

32. van der Pouw Kraan TC, Wijbrandts CA, van Baarsen LG, Voskuyl AE, Rustenburg F, Baggen JM, et al. Rheumatoid arthritis subtypes identified by genomic profiling of peripheral blood cells: assignment of a type I interferon signature in a subpopulation of patients. Ann Rheum Dis. 2007; 66(8):1008–14. https://doi.org/10.1136/ard.2006.063412 PMID: 17223656

33. Hassan M, Raslan HM, Eldin HG, Mahmoud E, Elwajed HAA. CD33(+) HLA-DR(-) Myeloid-Derived Suppressor Cells Are Increased in Frequency in the Peripheral Blood of Type1 Diabetes Patients with Predominance of CD14(+) Subset. Open Access Maced J Med Sci. 2018; 6(2):303–9. https://doi.org/10.3889/oamjms.2018.080 PMID: 29531593

34. Okano S, Abu-Elmagd K, Kish DD, Keslar K, Baldwin WM 3rd, Fairchild RL, et al. Myeloid-derived suppressor cells increase and inhibit donor-reactive T cell responses to graft intestinal epithelium in intestinal transplant patients. Am J Transplant. 2018; 18(10):2544–58. https://doi.org/10.1111/ajt.14718 PMID: 29509288

35. Martin P, Palmer G, Vigne S, Lamacchia C, Rodriguez E, Talabot-Ayer D, et al. Mouse neutrophils express the decoy type 2 interleukin-1 receptor (IL-1R2) constitutively and in acute inflammatory conditions. J Leukoc Biol. 2013; 94(4):791–802. https://doi.org/10.1189/jlb.0113035 PMID: 23817563

36. Shimizu K, Nakajima A, Sudo K, Liu Y, Mizoroki A, Ikarashi T, et al. IL-1 receptor type 2 suppresses collagen-induced arthritis by inhibiting IL-1 signal on macrophages. J Immunol. 2015; 194(7):3156–68. https://doi.org/10.4049/jimmunol.1402155 PMID: 25725107

37. Abboud S, Haile DJ. A novel mammalian iron-regulated protein involved in intracellular iron metabolism. J Biol Chem. 2000; 275(26):19906–12. https://doi.org/10.1074/jbc.M000713200 PMID: 10747949

38. Eash KJ, Greenbaum AM, Gopalan PK, Link DC. CXCR2 and CXCR4 antagonistically regulate neutrophil trafficking from murine bone marrow. J Clin Invest. 2010; 120(7):2423–31. https://doi.org/10.1172/JCI41649 PMID: 20516641

39. Manley HR, Keightley MC, Lieschke GJ. The Neutrophil Nucleus: An Important Influence on Neutrophil Migration and Function. Front Immunol. 2018; 9:2867. https://doi.org/10.3389/fimmu.2018.02867 PMID: 30564248

40. Shin JW, Spinler KR, Swift J, Chasis JA, Mohandas N, Discher DE. Lamins regulate cell trafficking and lineage maturation of adult human hematopoietic cells. Proc Natl Acad Sci U S A. 2013; 110(47):18892–7. https://doi.org/10.1073/pnas.1304996110 PMID: 24191023

41. Ouzounova M, Lee E, Piranlioglu R, El Andaloussi A, Kolhe R, Demirci MF, et al. Monocytic and granulocytic myeloid derived suppressor cells differentially regulate spatiotemporal tumour plasticity during metastatic cascade. Nat Commun. 2017; 8:14979. https://doi.org/10.1038/ncomms14979 PMID: 28382931

42. Goulart MR, Hlavaty SI, Chang YM, Polton G, Stell A, Perry J, et al. Phenotypic and transcriptomic characterization of canine myeloid-derived suppressor cells. Sci Rep. 2019; 9(1):3574. https://doi.org/10.1038/s41598-019-40285-3 PMID: 30837603

43. Cormier SA, Yuan S, Crosby JR, Protheroe CA, Dimina DM, Hines EM, et al. T(H)2-mediated pulmonary inflammation leads to the differential expression of ribonuclease genes by alveolar macrophages. Am J Respir Cell Mol Biol. 2002; 27(6):678–87. https://doi.org/10.1165/rcmb.4882 PMID: 12444027

44. Bosurgi L, Cao YG, Cabeza-Cabrerizo M, Tucci A, Hughes LD, Kong Y, et al. Macrophage function in tissue repair and remodeling requires IL-4 or IL-13 with apoptotic cells. Science. 2017; 356(6342):1072–6. https://doi.org/10.1126/science.aai8132 PMID: 28495875

45. Long EK, Hellberg K, Foncea R, Hertzel AV, Suttles J, Bernlohr DA. Fatty acids induce leukotriene C4 synthesis in macrophages in a fatty acid binding protein-dependent manner. Biochim Biophys Acta. 2013; 1831(7):1199–207. PMID: 24046860

46. Schachtrup C, Scholzen TE, Grau V, Luger TA, Sorg C, Spener F, et al. L-FABP is exclusively expressed in alveolar macrophages within the myeloid lineage: evidence for a PPARalpha-independent expression. Int J Biochem Cell Biol. 2004; 36(10):2042–53. https://doi.org/10.1016/j.biocel.2004.03.008 PMID: 15203117

47. Gibbings SL, Thomas SM, Atif SM, McCubbrey AL, Desch AN, Danhorn T, et al. Three Unique Interstitial Macrophages in the Murine Lung at Steady State. Am J Respir Cell Mol Biol. 2017; 57(1):66–76. https://doi.org/10.1165/rcmb.2016-0361OC PMID: 28257233

48. Zuo Y, d'Aigle J, Chauhan A, Frost JA. Genetic deletion of the Rho GEF Net1 impairs mouse macrophage motility and actin cytoskeletal organization. Small GTPases. 2017:1–8. https://doi.org/10.1080/21541248.2016.1197872 PMID: 27715453

49. Wojcik AJ, Skaflen MD, Srinivasan S, Hedrick CC. A critical role for ABCG1 in macrophage inflammation and lung homeostasis. J Immunol. 2008; 180(6):4273–82. https://doi.org/10.4049/jimmunol.180.6.4273 PMID: 18322240

50. Shayman JA, Tesmer JJG. Lysosomal phospholipase A2. Biochim Biophys Acta Mol Cell Biol Lipids. 2019; 1864(6):932–40. https://doi.org/10.1016/j.bbalip.2018.07.012 PMID: 30077006

51. Abe A, Hiraoka M, Wild S, Wilcoxen SE, Paine R, 3rd, Shayman JA. Lysosomal phospholipase A2 is selectively expressed in alveolar macrophages. J Biol Chem. 2004; 279(41):42605–11. https://doi.org/10.1074/jbc.M407834200 PMID: 15294901

52. Zhou Y, Do DC, Ishmael FT, Squadrito ML, Tang HM, Tang HL, et al. Mannose receptor modulates macrophage polarization and allergic inflammation through miR-511-3p. J Allergy Clin Immunol. 2018; 141(1):350–64 e8. https://doi.org/10.1016/j.jaci.2017.04.049 PMID: 28629744

53. Li D, Duan M, Feng Y, Geng L, Li X, Zhang W. MiR-146a modulates macrophage polarization in systemic juvenile idiopathic arthritis by targeting INHBA. Mol Immunol. 2016; 77:205–12. https://doi.org/10.1016/j.molimm.2016.08.007 PMID: 27541693

54. Morse C, Tabib T, Sembrat J, Buschur KL, Bittar HT, Valenzi E, et al. Proliferating SPP1/MERTK-expressing macrophages in idiopathic pulmonary fibrosis. Eur Respir J. 2019; 54(2):1802441. https://doi.org/10.1183/13993003.02441-2018 PMID: 31221805

55. Naito Y, Takagi T, Higashimura Y. Heme oxygenase-1 and anti-inflammatory M2 macrophages. Arch Biochem Biophys. 2014; 564:83–8. https://doi.org/10.1016/j.abb.2014.09.005 PMID: 25241054

56. Patsalos A, Tzerpos P, Halasz L, Nagy G, Pap A, Giannakis N, et al. The BACH1-HMOX1 Regulatory Axis Is Indispensable for Proper Macrophage Subtype Specification and Skeletal Muscle Regeneration. J Immunol. 2019; 203(6):1532–47. https://doi.org/10.4049/jimmunol.1900553 PMID: 31405954

57. Wammers M, Schupp AK, Bode JG, Ehlting C, Wolf S, Deenen R, et al. Reprogramming of pro-inflammatory human macrophages to an anti-inflammatory phenotype by bile acids. Sci Rep. 2018; 8(1):255. https://doi.org/10.1038/s41598-017-18305-x PMID: 29321478

58. Kusuyama J, Komorizono A, Bandow K, Ohnishi T, Matsuguchi T. CXCL3 positively regulates adipogenic differentiation. J Lipid Res. 2016; 57(10):1806–20. https://doi.org/10.1194/jlr.M067207 PMID: 27512010

59. Szondy Z, Sarang Z, Molnar P, Nemeth T, Piacentini M, Mastroberardino PG, et al. Transglutaminase 2-/- mice reveal a phagocytosis-associated crosstalk between macrophages and apoptotic cells. Proc Natl Acad Sci U S A. 2003; 100(13):7812–7. https://doi.org/10.1073/pnas.0832466100 PMID: 12810961

60. Toth B, Garabuczi E, Sarang Z, Vereb G, Vamosi G, Aeschlimann D, et al. Transglutaminase 2 is needed for the formation of an efficient phagocyte portal in macrophages engulfing apoptotic cells. J Immunol. 2009; 182(4):2084–92. https://doi.org/10.4049/jimmunol.0803444 PMID: 19201861

61. Yu X, Buttgereit A, Lelios I, Utz SG, Cansever D, Becher B, et al. The Cytokine TGF-beta Promotes the Development and Homeostasis of Alveolar Macrophages. Immunity. 2017; 47(5):903–12 e4. https://doi.org/10.1016/j.immuni.2017.10.007 PMID: 29126797

62. Lavin Y, Winter D, Blecher-Gonen R, David E, Keren-Shaul H, Merad M, et al. Tissue-resident macrophage enhancer landscapes are shaped by the local microenvironment. Cell. 2014; 159(6):1312–26. https://doi.org/10.1016/j.cell.2014.11.018 PMID: 25480296

63. Baitsch D, Bock HH, Engel T, Telgmann R, Muller-Tidow C, Varga G, et al. Apolipoprotein E induces antiinflammatory phenotype in macrophages. Arterioscler Thromb Vasc Biol. 2011; 31(5):1160–8. https://doi.org/10.1161/ATVBAHA.111.222745 PMID: 21350196

64. Zmijewski JW, Banerjee S, Abraham E. S-glutathionylation of the Rpn2 regulatory subunit inhibits 26 S proteasomal function. J Biol Chem. 2009; 284(33):22213–21. https://doi.org/10.1074/jbc.M109.028902 PMID: 19549781

65. Chen G, Tan CS, Teh BK, Lu J. Molecular mechanisms for synchronized transcription of three complement C1q subunit genes in dendritic cells and macrophages. J Biol Chem. 2011; 286(40):34941–50. https://doi.org/10.1074/jbc.M111.286427 PMID: 21862594

66. Verneret M, Tacnet-Delorme P, Osman R, Awad R, Grichine A, Kleman JP, et al. Relative contribution of c1q and apoptotic cell-surface calreticulin to macrophage phagocytosis. J Innate Immun. 2014; 6(4):426–34. https://doi.org/10.1159/000358834 PMID: 24557008

67. Osman R, Tacnet-Delorme P, Kleman JP, Millet A, Frachet P. Calreticulin Release at an Early Stage of Death Modulates the Clearance by Macrophages of Apoptotic Cells. Front Immunol. 2017; 8:1034. https://doi.org/10.3389/fimmu.2017.01034 PMID: 28878781

68. Mould KJ, Jackson ND, Henson PM, Seibold M, Janssen WJ. Single cell RNA sequencing identifies unique inflammatory airspace macrophage subsets. JCI Insight. 2019; 4(5):e126556. https://doi.org/10.1172/jci.insight.126556 PMID: 30721157

69. Nuncia-Cantarero M, Martinez-Canales S, Andres-Pretel F, Santpere G, Ocana A, Galan-Moya EM. Functional transcriptomic annotation and protein-protein interaction network analysis identify NEK2,

BIRC5, and TOP2A as potential targets in obese patients with luminal A breast cancer. Breast Cancer Res Treat. 2018; 168(3):613–23. https://doi.org/10.1007/s10549-017-4652-3 PMID: 29330624

70. Tang-Huau TL, Gueguen P, Goudot C, Durand M, Bohec M, Baulande S, et al. Human in vivo-generated monocyte-derived dendritic cells and macrophages cross-present antigens through a vacuolar pathway. Nat Commun. 2018; 9(1):2570. https://doi.org/10.1038/s41467-018-04985-0 PMID: 29967419

71. Porrello A, Leslie PL, Harrison EB, Gorentla BK, Kattula S, Ghosh SK, et al. Factor XIIIA-expressing inflammatory monocytes promote lung squamous cancer through fibrin cross-linking. Nat Commun. 2018; 9(1):1988. https://doi.org/10.1038/s41467-018-04355-w PMID: 29777108

72. Briseno CG, Haldar M, Kretzer NM, Wu X, Theisen DJ, Kc W, et al. Distinct Transcriptional Programs Control Cross-Priming in Classical and Monocyte-Derived Dendritic Cells. Cell Rep. 2016; 15 (11):2462–74. https://doi.org/10.1016/j.celrep.2016.05.025 PMID: 27264183

73. Sanyal R, Polyak MJ, Zuccolo J, Puri M, Deng L, Roberts L, et al. MS4A4A: a novel cell surface marker for M2 macrophages and plasma cells. Immunol Cell Biol. 2017; 95(7):611–9. https://doi.org/10.1038/icb.2017.18 PMID: 28303902

74. Hey YY, O'Neill TJ, O'Neill HC. A novel myeloid cell in murine spleen defined through gene profiling. J Cell Mol Med. 2019; 23(8):5128–43. https://doi.org/10.1111/jcmm.14382 PMID: 31210415

75. Segawa S, Kondo Y, Nakai Y, Iizuka A, Kaneko S, Yokosawa M, et al. Placenta Specific 8 Suppresses IL-18 Production through Regulation of Autophagy and Is Associated with Adult Still Disease. J Immunol. 2018; 201(12):3534–45. https://doi.org/10.4049/jimmunol.1800667 PMID: 30404814

76. Kuroda N, Masuya M, Tawara I, Tsuboi J, Yoneda M, Nishikawa K, et al. Infiltrating CCR2(+) monocytes and their progenies, fibrocytes, contribute to colon fibrosis by inhibiting collagen degradation through the production of TIMP-1. Sci Rep. 2019; 9(1):8568. https://doi.org/10.1038/s41598-019-45012-6 PMID: 31189971

77. Lim JK, Obara CJ, Rivollier A, Pletnev AG, Kelsall BL, Murphy PM. Chemokine receptor Ccr2 is critical for monocyte accumulation and survival in West Nile virus encephalitis. J Immunol. 2011; 186(1):471–8. https://doi.org/10.4049/jimmunol.1003003 PMID: 21131425

78. Coates BM, Staricha KL, Koch CM, Cheng Y, Shumaker DK, Budinger GRS, et al. Inflammatory Monocytes Drive Influenza A Virus-Mediated Lung Injury in Juvenile Mice. J Immunol. 2018; 200 (7):2391–404. https://doi.org/10.4049/jimmunol.1701543 PMID: 29445006

79. Bajpai G, Bredemeyer A, Li W, Zaitsev K, Koenig AL, Lokshina I, et al. Tissue Resident CCR2- and CCR2+ Cardiac Macrophages Differentially Orchestrate Monocyte Recruitment and Fate Specification Following Myocardial Injury. Circ Res. 2019; 124(2):263–78. https://doi.org/10.1161/CIRCRESAHA.118.314028 PMID: 30582448

80. Blasius AL, Cella M, Maldonado J, Takai T, Colonna M. Siglec-H is an IPC-specific receptor that modulates type I IFN secretion through DAP12. Blood. 2006; 107(6):2474–6. https://doi.org/10.1182/blood-2005-09-3746 PMID: 16293595

81. Zhang J, Raper A, Sugita N, Hingorani R, Salio M, Palmowski MJ, et al. Characterization of Siglec-H as a novel endocytic receptor expressed on murine plasmacytoid dendritic cell precursors. Blood. 2006; 107(9):3600–8. https://doi.org/10.1182/blood-2005-09-3842 PMID: 16397130

82. Grajkowska LT, Ceribelli M, Lau CM, Warren ME, Tiniakou I, Nakandakari Higa S, et al. Isoform-Specific Expression and Feedback Regulation of E Protein TCF4 Control Dendritic Cell Lineage Specification. Immunity. 2017; 46(1):65–77. https://doi.org/10.1016/j.immuni.2016.11.006 PMID: 27986456

83. Gueguen C, Bouley J, Moussu H, Luce S, Duchateau M, Chamot-Rooke J, et al. Changes in markers associated with dendritic cells driving the differentiation of either TH2 cells or regulatory T cells correlate with clinical benefit during allergen immunotherapy. J Allergy Clin Immunol. 2016; 137(2):545–58. https://doi.org/10.1016/j.jaci.2015.09.015 PMID: 26522402

84. Zimmermann HW, Bruns T, Weston CJ, Curbishley SM, Liaskou E, Li KK, et al. Bidirectional transendothelial migration of monocytes across hepatic sinusoidal endothelium shapes monocyte differentiation and regulates the balance between immunity and tolerance in liver. Hepatology. 2016; 63(1):233–46. https://doi.org/10.1002/hep.28285 PMID: 26473398

85. Cao W, Bover L, Cho M, Wen X, Hanabuchi S, Bao M, et al. Regulation of TLR7/9 responses in plasmacytoid dendritic cells by BST2 and ILT7 receptor interaction. J Exp Med. 2009; 206(7):1603–14. https://doi.org/10.1084/jem.20090547 PMID: 19564354

86. Bego MG, Miguet N, Laliberte A, Aschman N, Gerard F, Merakos AA, et al. Activation of the ILT7 receptor and plasmacytoid dendritic cell responses are governed by structurally-distinct BST2 determinants. J Biol Chem. 2019; 294(27):10503–18. https://doi.org/10.1074/jbc.RA119.008481 PMID: 31118237

87. Xing S, Li F, Zeng Z, Zhao Y, Yu S, Shan Q, et al. Tcf1 and Lef1 transcription factors establish CD8(+) T cell identity through intrinsic HDAC activity. Nat Immunol. 2016; 17(6):695–703. https://doi.org/10.1038/ni.3456 PMID: 27111144

88. Willinger T, Freeman T, Herbert M, Hasegawa H, McMichael AJ, Callan MF. Human naive CD8 T cells down-regulate expression of the WNT pathway transcription factors lymphoid enhancer binding factor 1 and transcription factor 7 (T cell factor-1) following antigen encounter in vitro and in vivo. J Immunol. 2006; 176(3):1439–46. https://doi.org/10.4049/jimmunol.176.3.1439 PMID: 16424171

89. Maier E, Hebenstreit D, Posselt G, Hammerl P, Duschl A, Horejs-Hoeck J. Inhibition of suppressive T cell factor 1 (TCF-1) isoforms in naive CD4+ T cells is mediated by IL-4/STAT6 signaling. J Biol Chem. 2011; 286(2):919–28. https://doi.org/10.1074/jbc.M110.144949 PMID: 20980261

90. Doucey MA, Goffin L, Naeher D, Michielin O, Baumgartner P, Guillaume P, et al. CD3 delta establishes a functional link between the T cell receptor and CD8. J Biol Chem. 2003; 278(5):3257–64. https://doi.org/10.1074/jbc.M208119200 PMID: 12215456

91. Borroto A, Lama J, Niedergang F, Dautry-Varsat A, Alarcon B, Alcover A. The CD3 epsilon subunit of the TCR contains endocytosis signals. J Immunol. 1999; 163(1):25–31. PMID: 10384095

92. Nechanitzky R, Akbas D, Scherer S, Gyory I, Hoyler T, Ramamoorthy S, et al. Transcription factor EBF1 is essential for the maintenance of B cell identity and prevention of alternative fates in committed cells. Nat Immunol. 2013; 14(8):867–75. https://doi.org/10.1038/ni.2641 PMID: 23812095

93. Luisiri P, Lee YJ, Eisfelder BJ, Clark MR. Cooperativity and segregation of function within the Ig-alpha/beta heterodimer of the B cell antigen receptor complex. J Biol Chem. 1996; 271(9):5158–63. https://doi.org/10.1074/jbc.271.9.5158 PMID: 8617796

94. Tedder TF, Streuli M, Schlossman SF, Saito H. Isolation and structure of a cDNA encoding the B1 (CD20) cell-surface antigen of human B lymphocytes. Proc Natl Acad Sci U S A. 1988; 85(1):208–12. https://doi.org/10.1073/pnas.85.1.208 PMID: 2448768

95. McHeyzer-Williams M, Okitsu S, Wang N, McHeyzer-Williams L. Molecular programming of B cell memory. Nat Rev Immunol. 2011; 12(1):24–34. https://doi.org/10.1038/nri3128 PMID: 22158414

96. Sheppard S, Schuster IS, Andoniou CE, Cocita C, Adejumo T, Kung SKP, et al. The Murine Natural Cytotoxic Receptor NKp46/NCR1 Controls TRAIL Protein Expression in NK Cells and ILC1s. Cell Rep. 2018; 22(13):3385–92. https://doi.org/10.1016/j.celrep.2018.03.023 PMID: 29590608

97. Bottcher JP, Bonavita E, Chakravarty P, Blees H, Cabeza-Cabrerizo M, Sammicheli S, et al. NK Cells Stimulate Recruitment of cDC1 into the Tumor Microenvironment Promoting Cancer Immune Control. Cell. 2018; 172(5):1022–37 e14. https://doi.org/10.1016/j.cell.2018.01.004 PMID: 29429633

98. Bade B, Boettcher HE, Lohrmann J, Hink-Schauer C, Bratke K, Jenne DE, et al. Differential expression of the granzymes A, K and M and perforin in human peripheral blood lymphocytes. Int Immunol. 2005; 17(11):1419–28. https://doi.org/10.1093/intimm/dxh320 PMID: 16186162

99. Pardo J, Balkow S, Anel A, Simon MM. Granzymes are essential for natural killer cell-mediated and perf-facilitated tumor control. Eur J Immunol. 2002; 32(10):2881–7. https://doi.org/10.1002/1521-4141(2002010)32:10<2881::AID-IMMU2881>3.0.CO;2-K PMID: 12355441

100. Turman MA, Yabe T, McSherry C, Bach FH, Houchins JP. Characterization of a novel gene (NKG7) on human chromosome 19 that is expressed in natural killer cells and T cells. Hum Immunol. 1993; 36(1):34–40. https://doi.org/10.1016/0198-8859(93)90006-m PMID: 8458737

101. Medley QG, Kedersha N, O'Brien S, Tian Q, Schlossman SF, Streuli M, et al. Characterization of GMP-17, a granule membrane protein that moves to the plasma membrane of natural killer cells following target cell recognition. Proc Natl Acad Sci U S A. 1996; 93(2):685–9. https://doi.org/10.1073/pnas.93.2.685 PMID: 8570616

102. Tian F, Han Y, Song J, Lei J, Yan X, Xie N, et al. Pulmonary resident neutrophils regulate the production of GM-CSF and alveolar macrophages. FEBS J. 2016; 283(8):1465–74. https://doi.org/10.1111/febs.13684 PMID: 26881904

103. Poole JA, Gleason AM, Bauer C, West WW, Alexis N, van Rooijen N, et al. CD11c(+)/CD11b(+) cells are critical for organic dust-elicited murine lung inflammation. Am J Respir Cell Mol Biol. 2012; 47(5):652–9. https://doi.org/10.1165/rcmb.2012-0095OC PMID: 22822029

104. Puttur F, Gregory LG, Lloyd CM. Airway macrophages as the guardians of tissue repair in the lung. Immunology and cell biology. 2019. https://doi.org/10.1111/imcb.12235 PMID: 30768869

105. Gibbons MA, Mackinnon AC, Ramachandran P, Dhaliwal K, Duffin R, Phythian-Adams AT, et al. Ly6Chi Monocytes Direct Alternatively Activated Pro-fibrotic Macrophage Regulation of Lung Fibrosis. American journal of respiratory and critical care medicine. 2011.

106. Laskin DL, Malaviya R, Laskin JD. Role of Macrophages in Acute Lung Injury and Chronic Fibrosis Induced by Pulmonary Toxicants. Toxicological sciences: an official journal of the Society of Toxicology. 2019; 168(2):287–301. https://doi.org/10.1093/toxsci/kfy309 PMID: 30590802

107. Bronte V, Brandau S, Chen SH, Colombo MP, Frey AB, Greten TF, et al. Recommendations for myeloid-derived suppressor cell nomenclature and characterization standards. Nat Commun. 2016; 7:12150. https://doi.org/10.1038/ncomms12150 PMID: 27381735

108. Damuzzo V, Pinton L, Desantis G, Solito S, Marigo I, Bronte V, et al. Complexity and challenges in defining myeloid-derived suppressor cells. Cytometry B Clin Cytom. 2015; 88(2):77–91. https://doi.org/10.1002/cyto.b.21206 PMID: 25504825

109. Karlson EW, Deane K. Environmental and gene-environment interactions and risk of rheumatoid arthritis. Rheum Dis Clin North Am. 2012; 38(2):405–26. https://doi.org/10.1016/j.rdc.2012.04.002 PMID: 22819092

110. Murphy D, Bellis K, Hutchinson D. Vapour, gas, dust and fume occupational exposures in male patients with rheumatoid arthritis resident in Cornwall (UK) and their association with rheumatoid factor and anti-cyclic protein antibodies: a retrospective clinical study. BMJ Open. 2018; 8(5):e021754. https://doi.org/10.1136/bmjopen-2018-021754 PMID: 29773705

111. Murphy D, Bellis K, Hutchinson D. Occupational dust and cigarette smoke exposure might link rheumatoid arthritis to COPD. Lancet Respir Med. 2018; 6(8):e36. https://doi.org/10.1016/S2213-2600(18)30188-7 PMID: 29759916

112. Murphy D, Hutchinson D. Is Male Rheumatoid Arthritis an Occupational Disease? A Review. Open Rheumatol J. 2017; 11:88–105. https://doi.org/10.2174/1874312901711010088 PMID: 28932330

113. Szema AM. Occupational Lung Diseases among Soldiers Deployed to Iraq and Afghanistan. Occup Med Health Aff. 2013;1. https://doi.org/10.4172/2329-6879.1000117 PMID: 24443711

114. Poole JA, Mikuls TR, Duryee MJ, Warren KJ, Wyatt TA, Nelson AJ, et al. A role for B cells in organic dust induced lung inflammation. Respir Res. 2017; 18(1):214. https://doi.org/10.1186/s12931-017-0703-x PMID: 29273051

115. Mortaz E, Alipoor SD, Adcock IM, Mumby S, Koenderman L. Update on Neutrophil Function in Severe Inflammation. Front Immunol. 2018; 9:2171. https://doi.org/10.3389/fimmu.2018.02171 PMID: 30356867

116. Rosales C. Neutrophil: A Cell with Many Roles in Inflammation or Several Cell Types? Front Physiol. 2018; 9:113. https://doi.org/10.3389/fphys.2018.00113 PMID: 29515456

117. Tsuda Y, Takahashi H, Kobayashi M, Hanafusa T, Herndon DN, Suzuki F. Three different neutrophil subsets exhibited in mice with different susceptibilities to infection by methicillin-resistant Staphylococcus aureus. Immunity. 2004; 21(2):215–26. https://doi.org/10.1016/j.immuni.2004.07.006 PMID: 15308102

118. Zhu J, Chen S, Wu L, Wang R, Zheng S, Zhao D, et al. The Expansion of Myeloid-Derived Suppressor Cells Is Associated with Joint Inflammation in Rheumatic Patients with Arthritis. Biomed Res Int. 2018; 2018:5474828. https://doi.org/10.1155/2018/5474828 PMID: 30046600

119. Fernandez IE, Greiffo FR, Frankenberger M, Bandres J, Heinzelmann K, Neurohr C, et al. Peripheral blood myeloid-derived suppressor cells reflect disease status in idiopathic pulmonary fibrosis. Eur Respir J. 2016; 48(4):1171–83. https://doi.org/10.1183/13993003.01826-2015 PMID: 27587556

120. Almand B, Clark JI, Nikitina E, van Beynen J, English NR, Knight SC, et al. Increased production of immature myeloid cells in cancer patients: a mechanism of immunosuppression in cancer. J Immunol. 2001; 166(1):678–89. https://doi.org/10.4049/jimmunol.166.1.678 PMID: 11123353

121. Bronte V, Serafini P, Apolloni E, Zanovello P. Tumor-induced immune dysfunctions caused by myeloid suppressor cells. J Immunother. 2001; 24(6):431–46. https://doi.org/10.1097/00002371-200111000-00001 PMID: 11759067

122. Melani C, Chiodoni C, Forni G, Colombo MP. Myeloid cell expansion elicited by the progression of spontaneous mammary carcinomas in c-erbB-2 transgenic BALB/c mice suppresses immune reactivity. Blood. 2003; 102(6):2138–45. https://doi.org/10.1182/blood-2003-01-0190 PMID: 12750171

123. Ohl K, Tenbrock K. Reactive Oxygen Species as Regulators of MDSC-Mediated Immune Suppression. Front Immunol. 2018; 9:2499. https://doi.org/10.3389/fimmu.2018.02499 PMID: 30425715

124. Groth C, Hu X, Weber R, Fleming V, Altevogt P, Utikal J, et al. Immunosuppression mediated by myeloid-derived suppressor cells (MDSCs) during tumour progression. Br J Cancer. 2019; 120(1):16–25. https://doi.org/10.1038/s41416-018-0333-1 PMID: 30413826

125. Sendo S, Saegusa J, Yamada H, Nishimura K, Morinobu A. Tofacitinib facilitates the expansion of myeloid-derived suppressor cells and ameliorates interstitial lung disease in SKG mice. Arthritis Res Ther. 2019; 21(1):184. https://doi.org/10.1186/s13075-019-1963-2 PMID: 31387650

126. Gordon S, Pluddemann A, Martinez Estrada F. Macrophage heterogeneity in tissues: phenotypic diversity and functions. Immunol Rev. 2014; 262(1):36–55. https://doi.org/10.1111/imr.12223 PMID: 25319326

127. Kielbassa K, Vegna S, Ramirez C, Akkari L. Understanding the Origin and Diversity of Macrophages to Tailor Their Targeting in Solid Cancers. Front Immunol. 2019; 10:2215. https://doi.org/10.3389/fimmu.2019.02215 PMID: 31611871

128. Wynn TA, Vannella KM. Macrophages in Tissue Repair, Regeneration, and Fibrosis. Immunity. 2016; 44(3):450–62. https://doi.org/10.1016/j.immuni.2016.02.015 PMID: 26982353

129. Rawlings DJ, Metzler G, Wray-Dutra M, Jackson SW. Altered B cell signalling in autoimmunity. Nat Rev Immunol. 2017; 17(7):421–36. https://doi.org/10.1038/nri.2017.24 PMID: 28393923

130. Hofmann K, Clauder AK, Manz RA. Targeting B Cells and Plasma Cells in Autoimmune Diseases. Front Immunol. 2018; 9:835. https://doi.org/10.3389/fimmu.2018.00835 PMID: 29740441

131. England BR, Duryee MJ, Roul P, Mahajan TD, Singh N, Poole JA, et al. Malondialdehyde-Acetaldehyde Adducts and Antibody Responses in Rheumatoid Arthritis-Associated Interstitial Lung Disease. Arthritis Rheumatol. 2019; 71(9):1483–93. https://doi.org/10.1002/art.40900 PMID: 30933423

132. Gianchecchi E, Delfino DV, Fierabracci A. NK cells in autoimmune diseases: Linking innate and adaptive immune responses. Autoimmun Rev. 2018; 17(2):142–54. https://doi.org/10.1016/j.autrev.2017.11.018 PMID: 29180124

133. Trouw LA, Pickering MC, Blom AM. The complement system as a potential therapeutic target in rheumatic disease. Nat Rev Rheumatol. 2017; 13(9):538–47. https://doi.org/10.1038/nrrheum.2017.125 PMID: 28794515

134. Botto M, Walport MJ. C1q, autoimmunity and apoptosis. Immunobiology. 2002; 205(4–5):395–406. https://doi.org/10.1078/0171-2985-00141 PMID: 12396002

135. Holers VM, Banda NK. Complement in the Initiation and Evolution of Rheumatoid Arthritis. Front Immunol. 2018; 9:1057. https://doi.org/10.3389/fimmu.2018.01057 PMID: 29892280

136. Gu H, Mickler EA, Cummings OW, Sandusky GE, Weber DJ, Gracon A, et al. Crosstalk between TGF-beta1 and complement activation augments epithelial injury in pulmonary fibrosis. FASEB J. 2014; 28(10):4223–34. https://doi.org/10.1096/fj.13-247650 PMID: 24958208

137. Gu H, Fisher AJ, Mickler EA, Duerson F 3rd, Cummings OW, Peters-Golden M, et al. Contribution of the anaphylatoxin receptors, C3aR and C5aR, to the pathogenesis of pulmonary fibrosis. FASEB J. 2016; 30(6):2336–50. https://doi.org/10.1096/fj.201500044 PMID: 26956419

138. Okamoto T, Mathai SK, Hennessy CE, Hancock LA, Walts AD, Stefanski AL, et al. The relationship between complement C3 expression and the MUC5B genotype in pulmonary fibrosis. Am J Physiol Lung Cell Mol Physiol. 2018; 315(1):L1–L10. https://doi.org/10.1152/ajplung.00395.2017 PMID: 29565179

139. Kulkarni HS, Liszewski MK, Brody SL, Atkinson JP. The complement system in the airway epithelium: An overlooked host defense mechanism and therapeutic target? J Allergy Clin Immunol. 2018; 141(5):1582–6 e1. https://doi.org/10.1016/j.jaci.2017.11.046 PMID: 29339260

140. Keith RC, Powers JL, Redente EF, Sergew A, Martin RJ, Gizinski A, et al. A novel model of rheumatoid arthritis-associated interstitial lung disease in SKG mice. Experimental lung research. 2012; 38(2):55–66. https://doi.org/10.3109/01902148.2011.636139 PMID: 22185348

141. Too CL, Muhamad NA, Ilar A, Padyukov L, Alfredsson L, Klareskog L, et al. Occupational exposure to textile dust increases the risk of rheumatoid arthritis: results from a Malaysian population-based case-control study. Ann Rheum Dis. 2016; 75(6):997–1002. https://doi.org/10.1136/annrheumdis-2015-208278 PMID: 26681695

142. Stolt P, Yahya A, Bengtsson C, Kallberg H, Ronnelid J, Lundberg I, et al. Silica exposure among male current smokers is associated with a high risk of developing ACPA-positive rheumatoid arthritis. Ann Rheum Dis. 2010; 69(6):1072–6. https://doi.org/10.1136/ard.2009.114694 PMID: 19966090

143. Nelson AJ, Roy SK, Warren K, Janike K, Thiele GM, Mikuls TR, et al. Sex differences impact the lung-bone inflammatory response to repetitive inhalant lipopolysaccharide exposures in mice. Journal of immunotoxicology. 2018; 15(1):73–81. https://doi.org/10.1080/1547691X.2018.1460425 PMID: 29648480